PERTURBED ANGULAR CORRELATION STUDIES IN PLATINUM

PERTURBED ANGULAR CORRELATION STUDIES IN PLATINUM

By

DAVID BEVAN KENYON, B.Sc.

A Thesis

Submitted to the Faculty of Graduate Studies

in Partial Fulfilment of the Requirements

for the Degree

Master of Science

McMaster University

June 1971

MASTER OF SCIENCE
(Physics)

McMASTER UNIVERSITY
Hamilton, Ontario

TITLE: Perturbed Angular Correlation Studies in Platinum

AUTHOR: David Bevan Kenyon, B.Sc. (McMaster University)

SUPERVISOR: Dr. J. A. Cameron

NUMBER OF PAGES: vi, 104

SCOPE AND CONTENTS:

Two isotopes of platinum, Pt^{192} and Pt^{194}, have been investigated using Ge(Li) vs. NaI coincidence techniques. The following corrected angular distributions and mixing ratios in Pt^{192} were obtained:

468-316 keV	$A_{22} = 0.100(8)$	$A_{44} = 0.011(8)$
604-316 keV	$A_{22} = -0.410(15)$	$A_{44} = -0.070(22)$
308-612 keV	$A_{22} = -0.120(20)$	$A_{44} = -0.027(20)$
417-468 keV	$A_{22} = -0.120(26)$	$A_{44} = -0.110(30)$

$$\delta_{308} = -9.4(15)$$

$$\delta_{604} = +3(1)$$

$$|\delta_{417}| > 11$$

g factors for the following five levels of these nuclei were obtained using the method of perturbed angular correlations where the perturbing agent was the hyperfine field on platinum in an iron alloy:

Pt^{192}	316 keV	g = 0.30(3)
Pt^{192}	612 keV	g = 0.28(7)
Pt^{192}	785 keV	g = 0.14(10)
Pt^{194}	329 keV	g = 0.28(3)
Pt^{194}	622 keV	g = 0.22(4)

A comparison with the predictions of a microscopic collective model, the pairing-plus-quadrupole model, is made.

TABLE OF CONTENTS

LIST OF FIGURES

LIST OF TABLES

TO MY PARENTS

CHAPTER I

INTRODUCTION

Since the first successful experiment was performed by Aeppli *et al* (1951), some 100 nuclear g factors have been measured by the various methods of perturbed angular correlations. The particular method applied in the present work, is a measurement of the angular displacement of a γ-γ directional correlation in a transverse magnetic field. The first experiment of this kind was reported by Frauenfelder *et al* (1954).

In the absence of any perturbation the γ-γ angular correlation, for any two γ-ray cascade, can be expressed as a series of even order Legendre polynomials:

$$W(\theta) = \sum_n A_{2n} P_{2n} (\cos\theta)$$

This correlation pattern may be altered if a perturbation is applied during the lifetime of the intermediate state. In particular, if this perturbation is a static magnetic field perpendicular to the plane of the γ-ray detectors, an angular displacement of the correlation may be observed. The effect of such a perturbation can be described semi-classically as a precession of the nuclear spin about the field direction.

It is this precession of the nucleus, while in the intermediate state, which gives rise to the angular displacement of the γ-γ directional correlation.

The magnitude of this displacement, and hence the feasibility of this method for obtaining g factors, is a function of the lifetime of the intermediate state and the size of the magnetic field acting on the nucleus. Practical considerations limit the conventional electromagnet to a useful field of about 50 k0e, and this implies that the mean life of the nuclear state to be studied must be greater than 100 picoseconds. However, by making use of the much larger hyperfine fields in ferromagnetic alloys, this lower limit on the mean life can be decreased to about 10 picoseconds.

Prior to 1961, all measurements were performed with external fields generated by electromagnets, and some 60 levels were studied in this way. Most of these levels were low energy single particle states in odd A nuclei and 2+ rotational states in even-even nuclei. With the introduction of the hyperfine field as the perturbing agent by Metzger (1961), it became possible to investigate much shorter lived states, including many 2+ vibrational states of even-even nuclei. To date some 30 additional levels have been studied in this manner, including the five of this investigation.

Kumar and Baranger (1968) have developed a pairing-plus-quadrupole description of these collective states, and

applied this model to the even-even isotopes of the near spherical nuclei, tungsten, osmium and platinum. Enough experimental g factors and other electromagnetic properties of these nuclei are now available that a meaningful comparison with this theory is possible.

CHAPTER II

THEORY OF THE METHOD

2.1 Angular Correlations

The probability of emission of a γ-ray by a nucleus is a function of the angle between the nuclear spin axis, and the direction of emission. Ordinarily, the total radiation from a radioactive sample is isotropic, since the nuclei are randomly oriented in space. To observe an anisotropic radiation pattern one must form an ensemble of nuclei that are not randomly oriented. This can be accomplished if the nuclei emit in rapid succession two γ-rays. The observation of the first γ-ray in a fixed direction selects an ensemble of nuclei that may have an anisotropic distribution of spin orientations. In other words, the magnetic substates of the intermediate level of the cascade may be unequally populated. The second γ ray of the cascade will then show a definite angular correlation with respect to the direction of the first.

A brief account of the theory of angular correlations will be made in the following paragraphs. The development outlined here is essentially that of Biedenharn and Rose (1953).

If we define $P_f(m_f)$ as being the probability of finding

the nucleus in the final state, m_f, while the two γ-rays, γ_1 and γ_2 , are observed in the directions $\bar{k}_1$ and $\bar{k}_2$, then the correlation function can be written

$$W(\bar{k}_1,\bar{k}_2) = \sum_{m_f} P_f(m_f)$$

Using the density matrix formalism, the probability, $P_f(m_f)$, is given by the diagonal elements of the density matrix for the final state.

$$W(\bar{k}_1,\bar{k}_2) = \sum_{m_f} \langle m_f|\rho_f(k_1,k_2)|m_f\rangle$$

This can be written in terms of the interaction, H_2, involved in the emission of the second γ ray of the cascade.

$$W(\bar{k}_1,\bar{k}_2) = S_2 \sum_{m_f m m'} \langle m_f|H_2|m\rangle\langle m|\rho(\bar{k}_1)|m'\rangle\langle m_f|H_2|m'\rangle^*$$

S_2 represents a summation over all unmeasured radiation properties, and $\langle m|\rho(\bar{k}_1)|m'\rangle$ is the density matrix for the intermediate state. This density matrix can be written

$$\langle m|\rho(\bar{k}_1)|m'\rangle = S_1 \sum_{m_i m_i'} \langle m|H_1|m_i\rangle\langle m_i|\rho_i|m_i'\rangle\langle m'|H_1|m_i'\rangle^*$$

$$= S_1 \sum_{m_i m_i'} \langle m|H_1|m_i\rangle\langle m'|H_1|m_i'\rangle$$

since the initial state is randomly oriented.

Substituting this result into the expression for $W(\bar{k}_1,\bar{k}_2)$ one

obtains:

$$W(\bar{k}_1,\bar{k}_2) = S_1 S_2 \sum_{m_f m m' m_i} \langle m_f|H_2|m\rangle\langle m|H_1|m_i\rangle\langle m'|H_1|m_i'\rangle^* \langle m_f|H_2|m'\rangle^*$$

It is convenient to express this in terms of a density operator for each transition:

$$W(\bar{k}_1,\bar{k}_2) = \sum_{mm'} \langle m|\rho(\bar{k}_1)|m'\rangle\langle m'|\rho(\bar{k}_2)|m\rangle$$

where

$$\langle m|\rho(\bar{k}_1)|m'\rangle = S_1 \sum_{m_i} \langle m|H_1|m_i\rangle\langle m'|H_1|m_i\rangle^*$$

and

$$\langle m'|\rho(\bar{k}_2)|m\rangle = S_2 \sum_{m_f} \langle m_f|H_2|m\rangle\langle m_f|H_2|m'\rangle^*$$

The problem now is to obtain expressions for matrix elements of the type $\langle m|H|m'\rangle$ and to combine them to form a more explicit expression for $W(\bar{k}_1,\bar{k}_2)$. To evaluate the matrix element $\langle m|H|m'\rangle \equiv \langle Imk\sigma|H|I'm'\rangle$ we transform from the plane wave representation, with quantum numbers $\bar{k}$ and σ (polarization), to the spherical representation, with quantum numbers L, M and π.

$$\langle Im\bar{k}\sigma|H|I'm'\rangle = \sum_{LM\pi} \langle \bar{k}\sigma|LM\pi\rangle\langle Im LM\pi|H|I'm'\rangle$$

The eigenfunctions $\langle \bar{k}\sigma|LM\pi\rangle$ are quantized along some arbitrary z axis, and can be expressed in terms of simpler eigenfunctions quantized along the direction of emission, k, by means of the

rotation matrix, $D^{L}_{\mu M} \equiv \langle \mu | D^{L} | M \rangle$.

$$\langle \bar{k}\sigma | LM\pi \rangle = \sum_{\mu} \langle O\sigma | L\mu\pi \rangle \; D^{L*}_{M\mu} \; (\alpha\beta\gamma)$$

The matrix element $\langle ImLM\pi | H | I'm' \rangle$ of the scalar operator H can be simplified by means of the Wigner Eckart theorem:

$$\langle ImLM\pi | H | I'm' \rangle = \langle ImLM | I'm' \rangle \langle I || L\pi || I' \rangle$$

Substituting these last two results into the expression for matrix elemnts of H in the plane wave representation, one obtains:

$$\langle m | H | m' \rangle = \sum_{L\pi M\mu} (-1)^{-I+L-m'} \begin{pmatrix} I & L & I' \\ m & M & -m' \end{pmatrix} \langle O\sigma | L\mu\pi \rangle$$

$$\times \langle I || L\pi || I' \rangle \; D^{L*}_{M\mu} \; (\alpha\beta\gamma)$$

Using this expression, one obtains a lengthy discussion for the matrix elements $\rho(\bar{k}_1)$:

$$\langle m | \rho(\bar{k}_1) | m' \rangle = S_1 \sum_{m_i} \langle m | H_1 | m_i \rangle \langle m' | H_1 | m_i \rangle^*$$

$$= S_1 \sum_{m_i} \sum_{L_1 M_1 \mu_1} \sum'_{k_1 N_1 \tau_1} \sum_{L_1' M_1' \mu_1'} (-1)^{M_1' - \mu_1'} (2k_1+1) \langle O_{\sigma_1} | L_1 \mu_1 \pi_1 \rangle$$

$$\times \langle O_{\sigma_1} | L_1' \mu_1' \pi_1' \rangle^* \begin{pmatrix} I & L_1 & I_1 \\ m & M_1 & -m_i \end{pmatrix} \begin{pmatrix} I & L_1' & I_i \\ m' & M_1' & -m_i \end{pmatrix} \begin{pmatrix} L_1 & L_1' & k_1 \\ M_1 & -M_1' & N_1 \end{pmatrix} \begin{pmatrix} L_1 & L_1' & k_1 \\ \mu_1 & -\mu_1' & \tau_1 \end{pmatrix}$$

$$\times \langle I || L_1 \pi_1 || I_i \rangle \langle I || L_1' \pi_1' || I_i \rangle^* \; D^{k_1}_{N_1 \tau_1} \; (\alpha\beta\gamma)$$

To obtain the above expression, use was made of the fact that the product of two matrix elements of the rotation group can be expressed in terms of a sum of matrix elements:

$$D^{L}_{\mu M}\, D^{L'}_{\mu' M'} = \sum_{k} \langle L\mu L'\mu' | k\tau \rangle \langle LML'M' | kN \rangle\, D^{k}_{\tau N}$$

where

$$N = M+M' \text{ and } \tau = \mu + \mu' \ .$$

Performing the sum over m_i, M_1 and M_1', and introducing the radiation parameters $C_{k_1\tau_1}(L_1L_1')$ one finally obtains:

$$m|\rho(\bar{k}_1)|m'\rangle = \sum_{L_1L_1'N_1\tau_1} (-1)^{2I-I_i+m-L_1'} (2k_1+1)^{1/2}\, C_{k_1\tau_1}(L_1L_1')$$

$$\times \begin{pmatrix} I & I & k_1 \\ m'-m & N_1 & \end{pmatrix} \begin{pmatrix} I & I & k_1 \\ L_1 L_1' & I_i & \end{pmatrix} \langle I||L_1\pi_1||I_i\rangle \langle I||L_1'\pi_1'|I_i\rangle^{*}\, D^{k_1}_{N_1\tau_1}(\alpha\beta\gamma)$$

where the parameters $C_{k_1\tau_1}$ are defined as:

$$C_{k_1\tau_1}(L_1L_1') = S_1 \sum_{\mu_1\mu_1'} (-1)^{L_1-\mu_1} (2k_1+1)^{1/2} \begin{pmatrix} L_1 & L_1' & k_1 \\ \mu_1 & -\mu_1' & \tau_1 \end{pmatrix} \langle O\sigma_1 | L_1\mu_1\pi_1\rangle^{*}$$

$$\times \langle O\sigma_1' | L_1'\mu_1'\pi_1'\rangle$$

These parameters are characteristic of the emitted radiation through the transformation coefficients $\langle O\sigma_1 | L_1\mu_1\pi_1\rangle$, and of the experimental arrangement through the averaging process designated by S_1.

Matrix elements of the density operator for the second

transition, $\langle m'|\rho(\bar{k}_2)|m\rangle$, are the same as those for the first transition except for phase and obvious changes in the subscripts.

Inserting the expressions for the two density matrices into the expression for $W(\bar{k}_1,\bar{k}_2)$ one obtains:

$$W(\bar{k}_1,\bar{k}_2) = (-1)^{2I-I_i-I_f} \sum_k \sum_{L_1L_1'L_2L_2'} \sum_{\tau_1\tau_2} (-1)^{k-L_1'-L_2'} \begin{Bmatrix} I & I & k \\ L_1 & L_1' & I_i \end{Bmatrix}$$

$$\times \begin{Bmatrix} I & I & k \\ L_2 & L_2' & I_f \end{Bmatrix} \langle I_f||L_2\pi_2||I\rangle\langle I_f||L_2'\pi_2'||I\rangle^* \langle I||L_1\pi_1||I_i\rangle$$

$$\times \langle I||L_1'\pi_1'||I_i\rangle^* \quad C_{k\tau_1}(L_1'L_1)\ C^*_{k\tau_2}(L_2L_2')\ D^k_{\tau_2\tau_1}$$

where

$$k = k_1 = k_2$$

and

$$N = N_1 = N_2 \ .$$

If one observes only the directions, and not the polarizations of the two radiations, then the correlation function is independent of the Euler angles γ_1 and γ_2 . This imples $\tau_1 = \tau_2 = 0$ and the representations D^k reduce to Legendre polynomials.

$$W(\theta) = \sum_k A_{kk}\ P_k(\cos\theta) \quad (k \text{ even})$$

The coefficients A_{kk} can be broken up into two factors, each a function of only one transition of the cascade:

$$A_{kk} = A_k(L_1L_1'I_iI)\ A_k(L_2L_2'I_fI)$$

where

$$A_k(L_1L_1'I_iI) = \sum_{L_1L_1'} (-1)^{L_1} C^*_{ko}(L_1L_1') \begin{Bmatrix} I & I & k \\ L_1 & L_1' & I_i \end{Bmatrix} \langle I||L_1\pi_1||I_i\rangle$$

$$\times \langle I||L_1'\pi_1'||I_i\rangle^*$$

and $A_k(L_2L_2'I_fI)$ differs only in subscripts.

The radiation parameters $C_{ko}(LL')$ have been calculated for γ-rays of mixed multipoles[†]. Substituting these into the above expression and introducing the coefficients F_k, we obtain:

$$A_k(L_1L_1'I_iI) = \frac{F_k(L_1L_1I_iI)+2\delta_1 F_k(L_1L_1'I_iI)+\delta_1^2 F_k(L_1'L_1'I_iI)}{1+\delta_1^2}$$

where

$$F_k(LL'I_iI) = (-1)^{I_i+I-1} [(2L+1)(2L'+1)(2I+1)(2k+1)]^{1/2} \begin{pmatrix} L & L' & k \\ 1 & -1 & 0 \end{pmatrix}$$

$$\times \begin{Bmatrix} L & L' & k \\ I & I & I_i \end{Bmatrix}$$

and the mixing ratio of the first transition is defined as the ratio of the reduced matrix elements

$$\delta_1 \equiv \frac{\langle I||L_1'\pi_1'||I_i\rangle}{\langle I||L_1\pi_1||I_i\rangle}$$

The coefficients $F_k(LL'I_iI)$ have been extensively tabulated by Ferentz and Rosenzweig (1954).

[†]Alpha, Beta and Gamma-Ray Spectroscopy, page 1029. Edited by K. Siegbahn (North-Holland Publishing Co.), 1966.

2.2 Perturbed Angular Correlations:

The correlation function developed to this point is valid only if the intermediate state is not changed before the emission of the second γ-ray of the cascade. Such a change is represented quantum-mechanically as a unitary transformation of the density operator for the intermediate state. This modification of the intermediate state can be the result of a magnetic or an electric field, and it is this effect that permits the determination of the g factor and quadrupole moment of certain excited states. The following paragraphs contain an outline of the theory of perturbed angular correlations first derived by Abragam and Pound (1953).

Using the notation of the previous section, the expression for the unperturbed angular correlation can be written:

$$W(\bar{k}_1,\bar{k}_2) = \sum_{m_i m_a m_b} \sum_{m_a' m_b' m_f} \langle m_f|H_2|m_b\rangle\langle m_a|H_1|m_i\rangle\, \delta_{m_a m_b}$$

$$\times \langle m_f|H_2|m_a'\rangle^*\langle m_b'|H_1|m_i\rangle^*\, \delta_{m_a' m_b'}$$

In this expression, H_1 and H_2 represent the interaction between the nucleus and the radiation field only. For the unperturbed correlation the final states $\langle m_a|$ and $\langle m_a'|$, after emission of the first γ-ray, are identical with the initial states $|m_b\rangle$ and $|m_b'\rangle$ of the second γ-ray.

We now apply a perturbation for the lifetime of the intermediate state which we describe by the Hamiltonian K.

During the time that this perturbation acts on the nucleus, the states $|m_a\rangle$ change to the states $|m_b\rangle$, and this change we represent by an unitary operator $\Lambda(t)$. The perturbed angular correlation can be expressed as:

$$W(\bar{k}_1,\bar{k}_2,t)= \sum_{m_i m_f} \sum_{m_a m_a} , \langle m_f|H_2\Lambda(t)|\, m_a\rangle\langle m_a|H_1|m_i\rangle\langle m_f|H_2\Lambda(t)|m_a'\rangle^*$$

$$\times \langle m_a'|H_1|m_i\rangle^*$$

This can be written in the form

$$W(\bar{k}_1,\bar{k}_2,t) = \sum_{m_f m_i} \sum_{m_a m_b} \sum_{m_a' m_b'} \langle m_f|H_2|m_b\rangle\langle m_b|\Lambda(t)|m_a\rangle$$

$$\times \langle m_a|H_1|m_i\rangle\langle m_f|H_2|m_b'\rangle^* \langle m_b'|\Lambda(t)|m_a'\rangle^*\langle m_a'|H_1|m_i\rangle^*$$

since

$$\Lambda(t)|m_a\rangle = \sum_{m_b} |m_b\rangle\langle m_b|\Lambda(t)|m_a\rangle$$

Introducing the density matrices of the previous section we get:

$$W(\bar{k}_1,\bar{k}_2,t) = \sum_{m_a m_a'} \sum_{m_b m_b'} \langle m_a|\rho(\bar{k}_1)|m_a'\rangle\langle m_b'|\rho(\bar{k}_2)|m_b\rangle$$

$$\times \langle m_b|\Lambda(t)|m_a\rangle\langle m_b'|\Lambda(t)|m_a'\rangle^*$$

Substituting the expressions for the density matrices derived in the previous section, and using the definition of the coefficients A_k, the perturbed angular correlation becomes:

$$W(\bar{k}_1,\bar{k},t) = \sum_{k_1 k_2 N_1 N_2} A_{k_1}(1) A_{k_2}(2)\, G^{N_1 N_2}_{k_1 k_2}(t)\, [(2k_1+1)(2k_2+1)]^{-1/2}$$

$$\times\, Y^{N_1 *}_{k_1}(\theta_1,\phi_1)\, Y^{N_2}_{k_2}(\theta_2,\phi_2)$$

The elements of the rotation matrix $D^{k}_{N\tau}$ have been expressed as spherical harmonics Y^{N}_{K}, since we have restricted the development to directional correlations (which implies $\tau=0$). The perturbation factor as defined in the above expression is:

$$G^{N_1 N_2}_{k_1 k_2}(t) = \sum_{m_a m_b} (-1)^{2I+m_a+m_b} [(2k_1+1)(2k_2+1)]^{1/2} \begin{pmatrix} I & I & k_1 \\ m_a' & -m_a & N_1 \end{pmatrix} \begin{pmatrix} I & I & k_2 \\ m_b' & -m_b & N_2 \end{pmatrix}$$

$$\times\, \langle m_b|\Lambda(t)|m_a\rangle \langle m_b'|\Lambda(t)|m_a'\rangle^*$$

The problem has been reduced to evaluating matrix elements of the evolution operator $\Lambda(t)$ for the particular perturbation of interest. In this development only the effect of a static magnetic field will be considered.

The Hamiltonian describing the interaction of a nuclear magnetic dipole moment μ with a fixed magnetic field $\bar{B}$ is:

$$K = -\bar{\mu}\cdot\bar{B} = -\mu_z B$$

where we have chosen the positive z axis in the direction of B. The energy eigenvalues are given by the diagonal elements of the Hamiltonian in the m-representation,

$$E_m = \langle I_m|K|I_m\rangle = -B\, \frac{m}{[(2I+1)(I+1)I]^{1/2}}\, \langle I||\mu||I\rangle$$

where we have applied the Wigner-Eckart theorem to remove the m dependence from the matrix elements. Using the usual definition of the magnetic moment μ, the expression for the energy eigenvalues becomes:

$$E_m = \frac{-B\mu m}{I} = \omega\hbar m$$

where ω is the Larmor frequency and given by:

$$\omega = \frac{-B\mu}{\hbar I} = -g\,\frac{\mu_N B}{\hbar}$$

The time dependent operator $\Lambda(t)$ must satisfy the Schrödinger equation:

$$\frac{\partial}{\partial t}\,\Lambda(t) = -\frac{i}{\hbar}\,K\Lambda(t)$$

Since we are dealing with a static magnetic field, the Hamiltonian K does not depend on time, and hence the solution of this equation is:

$$\Lambda(t) = \exp(-\frac{iKt}{\hbar}) = \exp(\frac{i\mu_z Bt}{\hbar})$$

As a result of the axial symmetry of the perturbing field, the evolution operator $\Lambda(t)$ and the Hamiltonian K are diagonal in the m-representation. Therefore we can write the matrix elements of this operator as:

$$\langle m_b|\Lambda(t)|m_a\rangle = \exp(-\frac{i}{\hbar}\,E_m t)\;\delta_{mm_a}\;\delta_{mm_b}$$

$$= \exp(-i\omega m t)$$

Substituting for the two matrix elements of the evolution operator, the perturbation factor becomes:

$$G^{NN}_{k_1k_2}(t) = \sum_m [(2k_1+1)(2k_2+1)]^{1/2} \begin{pmatrix} I & I & k_1 \\ -m & m' & N \end{pmatrix} \begin{pmatrix} I & I & k_2 \\ -m & m' & N \end{pmatrix} \exp(-iN\omega t)$$

$$= \exp(-iN\omega t)\,\delta_{k_1k_2}$$

Using this result, the expression for the perturbed angular correlation is:

$$W(\bar{k}_1,\bar{k}_2,t,B) = \sum_{N,k} A_k(1)A_k(2)\,\frac{1}{2k+1}\exp(-iN\omega t)Y^{N*}_k(\theta_1,\phi_1)Y^N_k(\theta_2,\phi_2)$$

If the γ-ray detectors are in the xy-plane, normal to the magnetic field direction, then $\theta_1 = \theta_2 = \frac{\pi}{2}$ and the angular correlation depends then only on the angle θ between the detectors.

$$W(\theta,t,B) = \sum_{N=0}^{N_{max}} b_{2N}\cos 2N(\theta-\omega t)$$

For the case $N_{max} = 2$, which is sufficient to describe all γ-γ perturbed angular correlations, the coefficients b_2 and b_4 are:

$$b_2 = \frac{\frac{3}{4}A_{22} + \frac{5}{16}A_{44}}{1 + \frac{1}{4}A_{22} + \frac{9}{64}A_{44}}$$

$$b_4 = \frac{\frac{35}{64}A_{44}}{1 + \frac{1}{4}A_{22} + \frac{9}{64}A_{44}}$$

If the resolving time of the coincidence system is much longer than the lifetime of the intermediate state, then a total time-integrated correlation is observed

$$W(\theta,B) = \frac{1}{\tau}\int_0^\infty [\sum_N b_{2N} \cos 2N(\theta-\omega t)]\, e^{-t/\tau}\, dt$$

$$= \sum_N \frac{b_{2N}}{1 + (2N\omega\tau)^2} (\cos 2N\theta - 2N\omega\tau \sin 2N\theta)$$

At this point it is convenient to introduce the quantity R, which we define as:

$$R = 2\,\frac{W(\theta,B) - W(\theta,-B)}{W(\theta,B) + W(\theta,-B)}$$

Substituting the above expression for $W(\theta,B)$, and noting that the second term changes sign as $B \to -B$, we get:

$$R = \frac{-2 \sum_N \frac{b_{2N}}{1+(2N\omega\tau)^2} 2N\omega\tau \sin 2N\theta}{\sum_N \frac{b_{2N}}{1+(2n\omega\tau)^2} \cos 2N\theta}$$

If we make the assumption that $\omega\tau << 1$, then R becomes:

$$R = 2\omega\tau \left[\frac{1}{W(\theta)} \frac{\partial W(\theta)}{\partial\theta}\right]$$

The experimental procedure is to measure the unperturbed directional correlation $W(\theta)$ and hence obtain its logarithmic derivative $\frac{1}{W(\theta)} \frac{\partial W(\theta)}{\partial\theta}$, and then to measure this quantity R. As defined above $\frac{R}{2}$ is simply the coincident count rate observed with the transverse field in one direction, minus that

observed with the field direction reversed, divided by the sum of the two rates. These two measurements yield a value for the rotation of the intermediate state $\omega\tau$, and if the mean life of the state is known, the Larmor precession frequency follows. The magnetic moment (g factor) of this state can then be calculated if the magnitude of the magnetic field acting on the nucleus is known.

2.3 Hyperfine Fields

The magnetic field acting on an impurity nucleus in a ferromagnetic host can be represented as the sum of two terms; an external field due to the experimental arrangement and an internal field which arises as a result of the ferromagnetic host.

$$\bar{H} = \bar{H}_{ext} + \bar{H}_{int}$$

In practice the first term is so much smaller than the second that it can be safely ignored, and the perturbing field can be considered to be an entirely internal effect.

According to Marshall (1958) this internal field can be broken up into three factors:

$$\bar{H}_{int} = \bar{H}_{hyp} - D\bar{M} + \frac{4\pi}{3}\bar{M}$$

The first term is the hyperfine field and is a result of the interaction between the nucleus and the atomic electrons. The

second term reflects the geometry of the sample through the demagnetizing factor D. The last term is the Lorentz field for a cubic lattice. For a given sample the field due to the last two terms can be calculated, and for impurity atoms in iron is much less than the measured effective field.

In ferromangetic alloys in which iron is the host, the hyperfine field on metallic impurities is thought to be the result of the s-electrons of the impurity atom being spin-polarized by the d-electrons of iron. This polarization can be caused by an exchange force between the s-electrons of the impurity and the d-electrons of iron, or by the admixture of the s-electrons into the unfilled 3d-shell. The field generated by the interaction of polarized s-electrons with the impurity nucleus in a dilute alloy is large and negative (in excess of 1000 k0e for impurities in the z=78 region).

For dilute iron alloys, that is for impurity concentrations of less than a few atomic percent, Kontani and Itoh (1967) have shown that the magnitude of the hyperfine field acting on the impurity nucleus is not a function of the concentration. For larger impurity concentrations the value of this field is not unique.

Values for the hyperfine field have been measured for many dilute iron alloys by means of nuclear magnetic resonance experiments. Since these measurements are performed at a very much lower temperature than those of this investigation, a

correction to the value quoted for the hyperfine field is necessary. Nagle et al. (1960) have investigated the temperature dependence of the hyperfine field on iron in iron and found it to be proportional to the saturation magnetization. The temperature dependence of the saturation magnetization to first order is given by:

$$\frac{\Delta M}{M(O)} = KT^{3/2}$$

where K is a constant independent of temperature and the change in saturation magnetization ΔM is defined as:

$$\Delta M \equiv M(O) - M(T)$$

This expression due to Block (1931) is known as the Block $T^{3/2}$ Law, and is a first order result of spin wave theory. The constant K has been assigned an experimental value of $(3.4\pm0.2)\times10^{-6}$ deg.$^{-3/2}$ for iron by Argyle et al. (1963).

CHAPTER III

THE APPARATUS

3.1 Angular Correlations

Measurements of the unperturbed angular correlation $W(\theta)$ are performed using three detectors mounted on an automatic table. The two moveable detectors are 2" by 2" NaI crystals integrally mounted to RCA 6342A photomultiplier tubes. The bases for these tubes were supplied by Ortec (model 269). The fixed detector is a 25 cc. Ge(Li) detector (Nuclear Diodes) with a resolution of approximately 1% at 300 keV for high count rates (greater than 10^4 events/sec).

The angular correlation table is constructed entirely of aluminum and consists of a 4' by 2-1/2' table surface in the centre of which is mounted a small micrometer table (2-1/2" by 2-1/2"), the arms upon which the detectors are mounted, and a motor and associated pulleys and bearings necessary to move one of the detector arms. Mounted on the small micrometer table is a brass cup used to hold either a lucite source holder (for an angular correlation measurement) or a small electromagnet (for a perturbed measurement). This small table can be moved 1/4" in any direction away from the centre of the angular correlation table with an accuracy of ±1

thousandths of an inch. It is this micrometer table which permits centering of the source relative to the three detectors. Mounted on the end of the motor driven arm is a solenoid operated pin. Beneath the path traced out by this pin five holes have been drilled in the table at 22-1/2° intervals. As the detector arm is moved the pin drops into one of these holes and the arm remains at that angle until the pin is raised. To perform am angle change then, the pin solenoid is activated for about 1/2 second and the motor is switched on for another five seconds. Since the motor is reversible, this detector arm can be moved from the 90° position to the 180° position and then back again to the 90° position in ten steps (the 90° position is defined as that position of the arm for which the angle between the fixed detector and the detector labelled #2 is 90°). Since only one of the arms is driven directly by the motor, during a measurement of $W(\theta)$ the two moveable arms are fixed together with an angular separation of 90°.

A block diagram of a part of the associated electronics is shown in Figure 1. The preamplifiers for the NaI detectors are Ortec scintillation preamps (model 113) while a charge sensitive Ortec 118A is used with the Ge(Li) detector. All three channels contain active filter pulse amplifiers (Ortec 440A) and two timing single channel analyzers (Canberra model 1436). Fast coincidences are performed as shown by two EG+G C102B/N modules. The four coincidence outputs are buffered

Figure 1: Block diagram of the electronics. During a measurement of an angular correlation, the coincidence rate is monitored as a function of the angle θ. The two moving detectors, 2 and 3, are fixed with an angular separation of 90°. With the SCA's selecting the γ-rays as shown, the correlation function for cascade A-C appears at the outputs labelled 2 and 4, while that for the cascade D-B appears at those labelled 1 and 3.

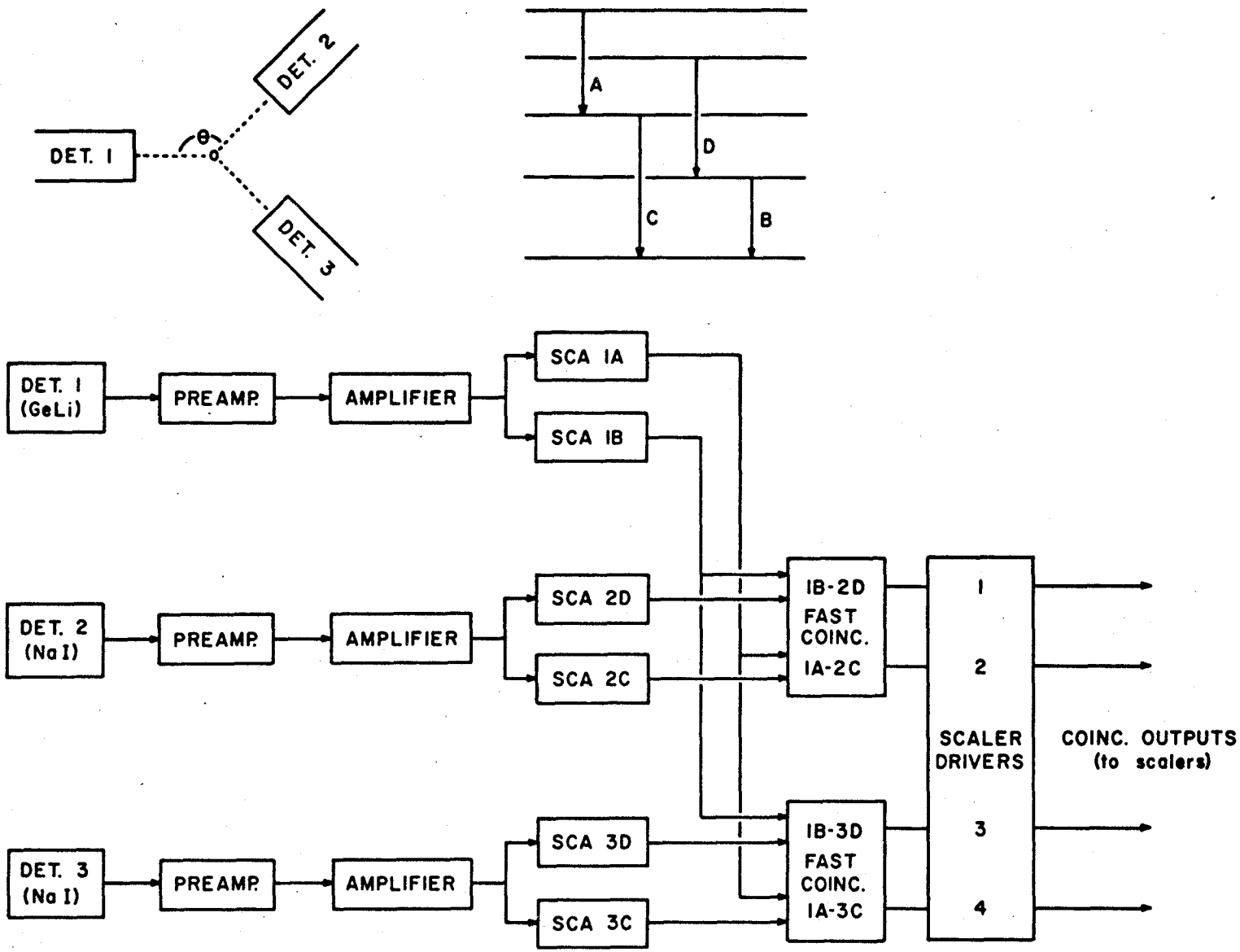
DET. 1
DET. 2
DET. 3
θ
A
D
C
B
DET. 1 (GeLi)
PREAMP.
AMPLIFIER
SCA 1A
SCA 1B
DET. 2 (Na I)
PREAMP.
AMPLIFIER
SCA 2D
SCA 2C
DET. 3 (Na I)
PREAMP.
AMPLIFIER
SCA 3D
SCA 3C
1B-2D FAST COINC. 1A-2C
1B-3D FAST COINC. 1A-3C
SCALER DRIVERS
1
2
3
4
COINC. OUTPUTS (to scalers)

by means of four scalar drivers contained in an EG+G DS104/N module. These four buffered outputs are connected to the inputs of four of the six scalers in the programmer (to be described in a later section of this chapter).

During a measurement of $W(\theta)$ the four coincidence count rates are monitored as a function of the angle between the fixed detector and either of the two moveable detectors. In some of the experiments of this investigation the correlation patterns for two cascades were measured simultaneously. To accomplish this, the two SCA's in the Ge(Li) channel were set to select the lower energy γ-ray of each cascade (A and B in Figure 1). The SCA's in the two NaI channels were adjusted to select the higher energy γ-rays of each cascade (C and D) as shown in Figure 1. With the electronics set up in this fashion, the correlation function for the cascade A-C was observed at the outputs labelled 2 and 4, while that for the cascade D-B appeared at those labelled 1 and 3.

Since the gain of a photomultiplier tube is a function of the high voltage supplied to that tube, some form of stabilization is necessary to ensure long term pulse height stability. One method for achieving this stability is to use an expensive well regulated high voltage supply. However this method does not correct for any gain changes which might occur in the associated preamplifier or amplifier. A much better method is to use a cheap, not so well regulated supply

and a single channel analyzer. This SCA is set to select a prominent photopeak in the spectrum (or a peak generated by a light pulser). The baseline of this window is square wave modulated so that the window is swept back and forth across the peak. The integrated count rate on each side of the peak is compared and an appropriate correction signal is generated and applied to the high voltage supply. If for example, the count rate was higher on the high energy side of the peak, the correction signal would be such as to reduce the high voltage, lowering the gain of the photomultiplier. This would bring the peak back into the middle of the region swept out by the window. This method is sensitive to any gain changes which might occur in the photomultiplier or its associated electronics, and through its use pulse height stability can be achieved for an indefinite period of time.

A high voltage power supply with a built in stabilization SCA is available from Cosmic Radiation Labs (model 1001) and three such supplies were used to bias the three detectors. The stabilization circuit was disabled on the supply which was biasing the Ge(Li) detector, since this type of detector is not sensitive to bias voltage fluctuations.

3.2 Perturbed Angular Correlations

Once the angular correlation function $W(\theta)$ has been measured and the position of maximum slope $\frac{\partial W}{\partial \theta}$ established, the magnetic measurements can be made. The electromagnet used

in a perturbed run does not possess cylindrical symmetry and hence it cannot be used to hold the source for a measurement of $W(\theta)$.

The magnet consists of two coils, each of 500 turns of #20 copper wire, a mild steel yoke, and water cooled end plates. The yoke has a 1" diameter hole cut out of one side and a 1" high slit of angular length 130° in the other side to allow the detectors an unobstructed view of the source. This magnet generates 1 k0e per ampere within a 1/2 cm. gap. The magnet current is supplied by a 20 volt, 20 amp. power supply from Harrison Labs (model 6264A). Surrounding the pole tips, which screw down upon the source, is a lucite annulus with an outer diameter of 1". This lucite ring, together with the μ-metal detector shield, reduces the β-ray flux at the detectors to an insignificant level.

The stray magnetic field acting on the photomultiplier tubes was reduced to less than 5 milligauss by a 20 turn bucking coil wound around the outside of the yoke of the magnet and by magnetic shields placed around the tubes. The current in the bucking coil is a variable fraction of the magnet current, and the best value for this fraction is established by observing the stray magnetic field with a Hall probe incremental gaussmeter (Bell model 640). The magnetic shields were formed by wrapping sheets of Conetic AA, high permeability steel, around the photomultiplier tubes.

During a perturbed run the detectors are fixed at the position of maximum slope of the angular correlation function $W(\theta)$. The electronics of figure 1 is unchanged from that used during a measurement of $W(\theta)$. The source is placed between the pole tips of the electromagnet and the change in coincidence count rate is observed as the field direction is reversed. In a three detector system the definition of R (section 2.2) becomes:

$$\frac{R}{2} = \frac{[W(\theta,H)+W(-\theta,-H)] - [W(\theta,-H)+W(-\theta,H)]}{[W(\theta,H)+W(-\theta,-H)] + [W(\theta,-H)+W(-\theta,H)]}$$

$$\text{since } W(\theta,H) = W(-\theta,-H)$$

Thus for a particular field direction the coincidence output labelled 1 is equivalent to that labelled 3 when the field direction is reversed. A similar relationship exists between the outputs labelled 2 and 4. With the field in one direction, the outputs labelled 1, 2, 3 and 4 are connected to scalers 1, 2, 3 and 4 respectively. When this field direction is reversed, the outputs labelled 1, 2, 3 and 4 are directed to scalers 3, 4, 1 and 2 respectively. As defined above then, R/2 for one cascade is simply the total number of counts in scaler 1 minus that of scaler 3 divided by the sum of the two. The contents of scalers 2 and 4 yield R/2 for the other cascade in a similar manner.

The field direction is reversed every 10 seconds to reduce systematic effects such as fluctuations in pulse height and resolving time. Theoretically, if these fluctuations are not correlated with the switching cycle, these systematic errors can be eliminated entirely by switching at a very high rate. However, in practice the scalers are stopped for approximately 1/6 second during each switch to prevent the counting of switching transients, and the dead time becomes appreciable for switching rates higher than one every 10 seconds.

When the alloy source consists of a ferromagnetic host with a Curie temperature below that of liquid nitrogen, a special low temperature apparatus is used (McMath, 1967). Although this apparatus was not used in the experiments described in this report, mention of it is made here because numerous references will be made to it in a later section and in the appendix. The source is placed in a small superconducting magnet (17 kOe) which is immersed in a dewar containing liquid helium. Surrounding this dewar is a jacket of liquid nitrogen. While it is possible to reverse the iron magnet field direction every few seconds, several minutes are required to do so with the superconducting magnet. The current through the superconducting coil must be changed slowly to prevent it from returning to the normal state. The

power supply for this magnet (same unit as is used with the iron magnet) is externally programmed by a ten turn precision potentiometer. This potentiometer is in turn controlled by a 1 rpm reversible motor. To perform a switch in field direction with this magnet, the current through the coil is first slowly reduced to zero by this motor, the magnet polarity is reversed, and the current is raised slowly back up to operating level (typically 15 amperes).

3.3 The Programmer

A digital system has been constructed to control the experiment and to collect and periodically output the data. It can be thought of as consisting of two subsystems; one contains the logic necessary to control three experiements, an angular correlation (AC), a perturbed angular correlation (PAC) using the iron magnet (IM), and a PAC using the superconducting magnet (SCM). The other subsystem contains six 24 bit BCD scalers, the necessary input gating, and a typewriter readout control. A simplified block diagram is shown in Figure 2, and a brief description is made in the following paragraphs. A considerably more detailed description of this system, complete with schematics and wiring schedule, is contained in Appendix I.

Except for pulse amplifiers and solenoid drivers, this system is constructed entirely of integrated circuits (MDTL by

Figure 2: Block diagram of the programmer.

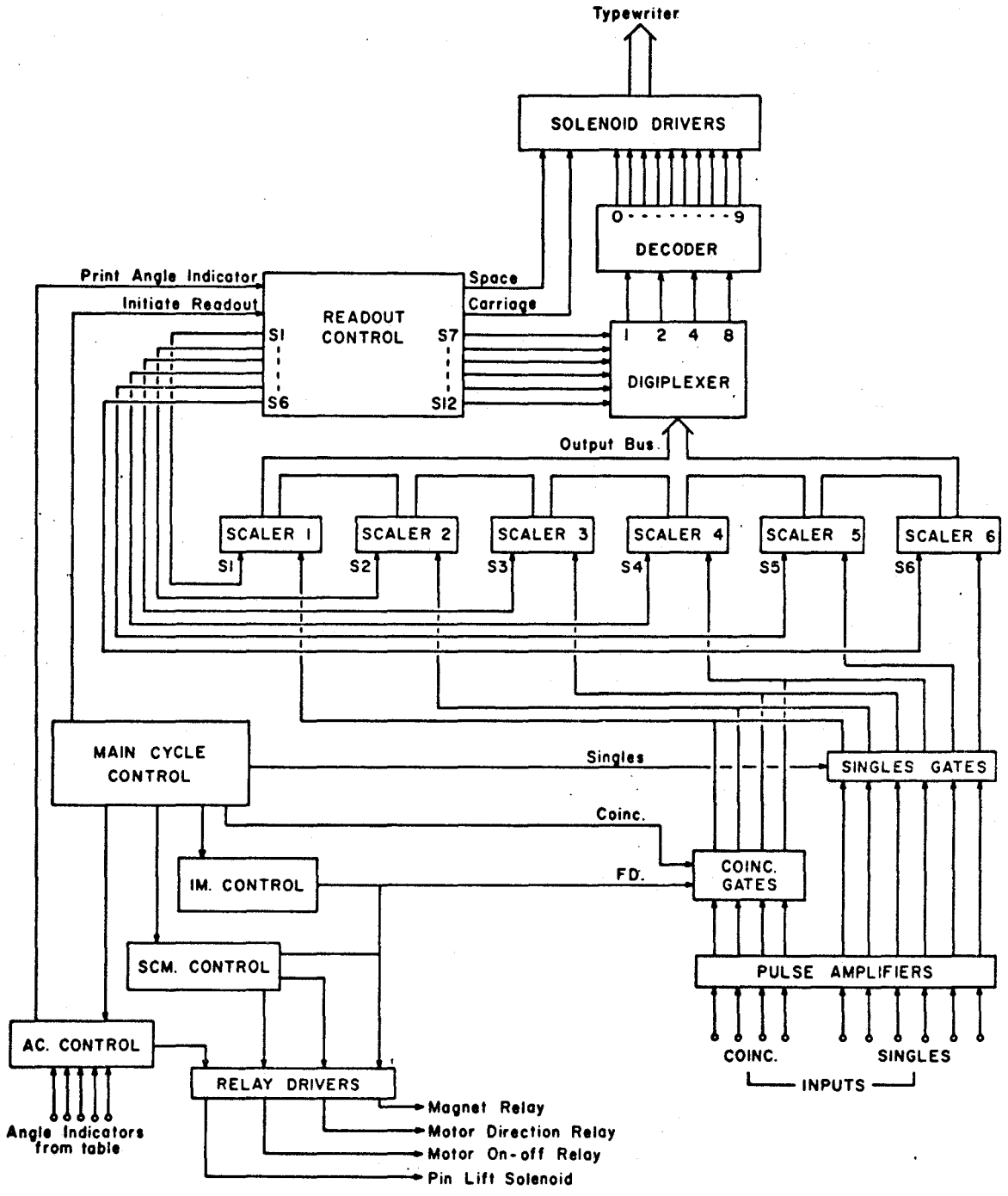
Typewriter
SOLENOID DRIVERS
0 - - - - - - - - 9
DECODER
Print Angle Indicator
Initiate Readout
READOUT CONTROL
S1
S6
S7
S12
Space
Carriage
1 2 4 8
DIGIPLEXER
Output Bus
SCALER 1
SCALER 2
SCALER 3
SCALER 4
SCALER 5
SCALER 6
S1
S2
S3
S4
S5
S6
MAIN CYCLE CONTROL
Singles
SINGLES GATES
Coinc.
IM. CONTROL
FD.
COINC. GATES
SCM. CONTROL
PULSE AMPLIFIERS
AC. CONTROL
RELAY DRIVERS
COINC.
SINGLES
INPUTS
Angle Indicators from table
Magnet Relay
Motor Direction Relay
Motor On-off Relay
Pin Lift Solenoid

Motorola). While DTL logic is comparatively slow, it exhibits excellent noise immunity and can be used to perform the wired-OR function .

The pulses which appear at the ten inputs, four coincidence and six singles, are inverted by transistor amplifiers. The purpose of these amplifiers is to limit the pulse height to +5 volts, and to shorten the fall time of the pulse. The six singles signals are inverted and then gated by the signal labelled Singles. The four coincidence lines are inverted and then gated by the signal labelled Coinc. They are further gated by the signal F.D. (field direction) in the following manner: with the signal F.D. high (+5 volts) the inputs labelled 1, 2, 3 and 4 are routed to scalers 1, 2, 3 and 4 respectively. When the signal F.D. is low, these inputs are routed to scalers 2, 1, 4 and 3 respectively. After this gating, the four coincidence lines are OR'ed with the first four singles lines to the inputs of scalers 1 to 4. Singles lines 5 and 6 are the only inputs of scalers 5 and 6.

Scalers 1 to 4 are identical and differ from 5 and 6 only in clear mechanism. They are all 40 Mcs, 24 bit BCD scalers containing six IC decade counters (MC838P). A Schmidt trigger on the input generates the fast fall time required ($\sim$ 20 ns) to trigger the least significant decade counter. All 24 output lines are gated and inverted. These gated outputs from all

six scalers are OR'ed and become inputs of a digiplexer. The contents of scalers 1 to 6 are presented to this digiplexer as strobe lines S1 to S6 come high. The digiplexer presents one digit (four bits) to the BCD to decimenal decoder depending upon which of the six strobe lines labelled S7 to S12 is high. The ten outputs of the decoder are amplified and then used to drive the 0 to 9 solenoids of an IBM typewriter.

The six digit strobes (S7 to S12) are generated by the more significant six bits of a seven bit ring counter. The six scaler strobes (S1 to S6) are generated by a six bit shift register. Each time the ring counter overflows this shift register is advanced one bit. When the shift register overflows a carriage return is generated and readout of the six scalers is complete. Readout control also contains the logic necessary to suppress leading zeros.

The block labelled MAIN CYCLE CONTROL contains the system clock and the interface with all switches on front and rear panels. This block determines which of the three cycles is to be run (AC, IM or SCM) and provides certain signals to the appropriate control block. Main cycle control is also responsible for opening the coincidence gates or the singles gates and for initiating a readout of the six scalers. The system clock is a 1 Mc crystal controlled oscillator which is scaled down to 100 cps by decade counters, and then further scaled by a 20 bit binary counter. The outputs of this 20 bit

scaler are directed to several tap switches on the front panel. The selected signals are shaped by monostables and used as various control signals.

Regardless of which experiment is in progress (AC, IM or SCM) the same main program is executed. An outline of this main program is shown below:

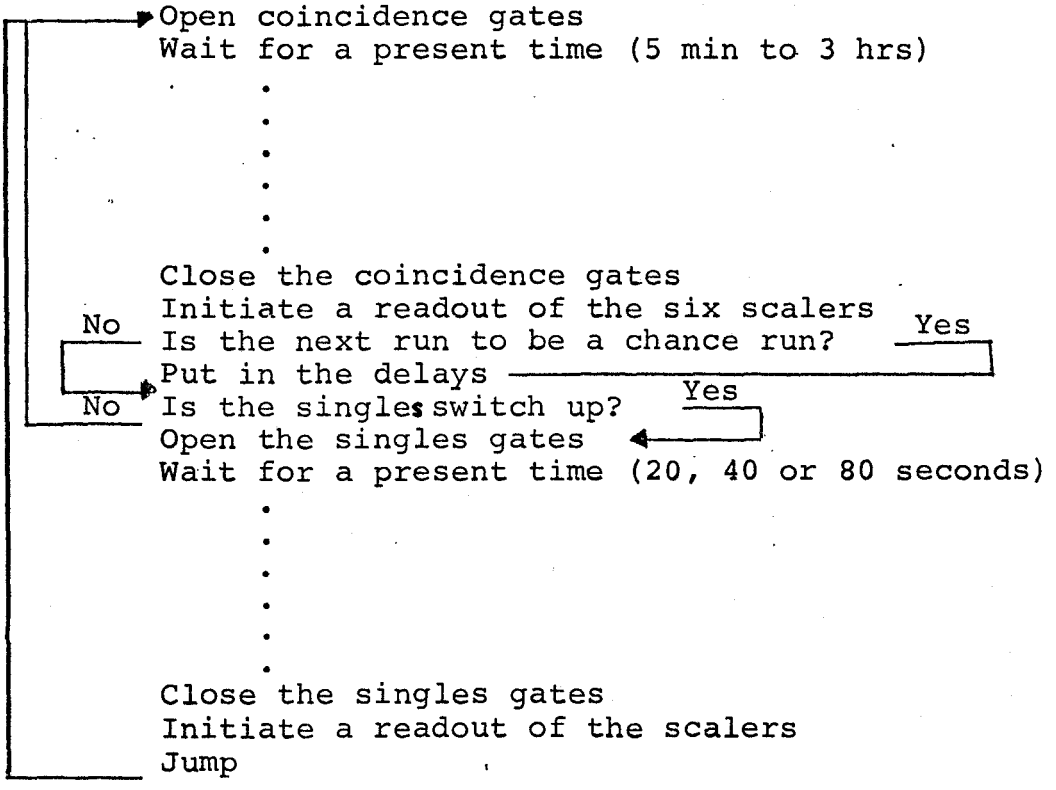

The specific programs used to control the three types of experiment are generated by adding small subprograms to this main program. These smaller subprograms are generated by the AC, IM and SCM CONTROL blocks, and they are selected by means of several front panel switches. The main program

and the subprogram are executed simultaneously. The IM subprogram is executed from the time the coincidence gates are opened until the time they are closed, while the AC and SCM subprograms are executed during the time that these gates are closed. The three subprograms are outlined below:

AC Subprogram

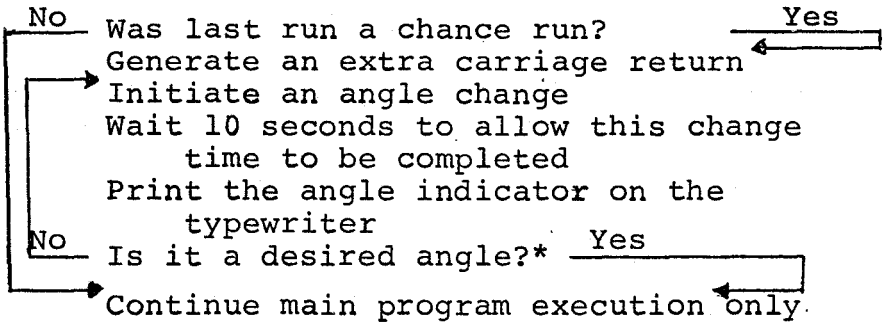

*The angular correlation table has five possible positions from 90° to 180° in steps of 22-1.2°. Coresponding to these five angles are five switches on the rear panel of the programmer. Those switches which are in the up position indicate which of the angles are desired.

IBM Subprogram

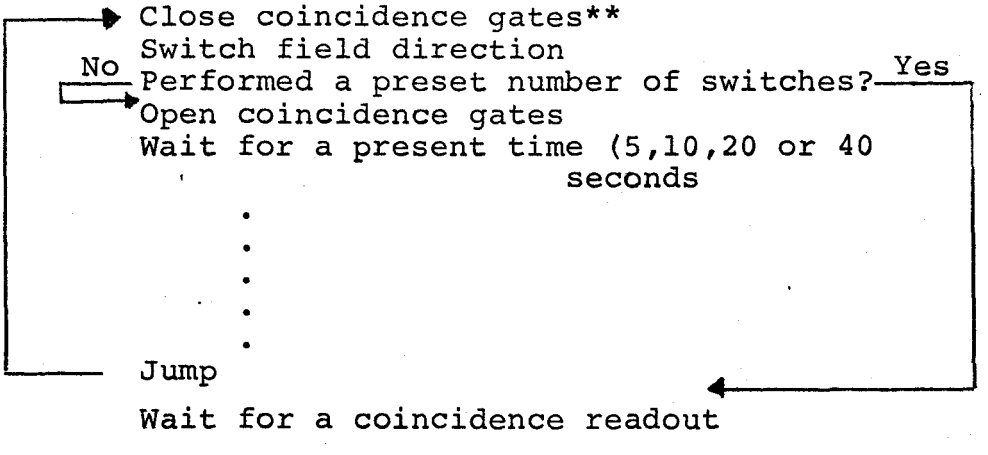

**The coincidence gates are closed during the reversal of the iron magnet field direction to prevent switching transients from being counted by the scalers.

SCM Subprogram	Switch motor direction to down*
	Turn on motor
	Wait for a preset time (20,40, or 80 seconds)
	Turn off motor
	Switch motor direction to up
	Switch superconducting magnet field direction
	Turn on motor
	Wait for a preset time (20,40 or 80 seconds)
	Turn off motor
	Resume main program execution only

*This motor is the 1 rpm reversible motor used to drive a ten turn potentiometer. The superconducting magnet power supply is externally programmed by the potentiometer.

CHAPTER IV

THE EXPERIMENTS

4.1 Introduction

The experiments to be described in this chapter involve the first three excited states of Pt^{192} and the first two of Pt^{194}. The magnetic moments of all but one of these levels, the 4+ in Pt^{192}, had been previously measured using scintillation detectors (Agarwal et al, 1965; Keszthelyi et al, 1965; Murray, 1967). In deriving the true angular distributions for all cascades, and the g factors for the second 2+ states, substantial corrections due to unresolved γ-rays were necessary. Many of these corrections can be avoided by taking advantage of the resolution of a Ge(Li) detector, and it was to this end that this work was undertaken. The derivation of g factors for the first 2+ levels in both nuclei is free of these corrections and hence those values obtained using scintillation detectors are considered to be reliable. They were remeasured in this investigation only to provide a check of the apparatus.

In the sections that follow, an outline of the experimental procedure is made and the results are presented. Unless otherwise noted, the procedure used in the study of the levels of Pt^{194} was identical with that used for Pt^{192}.

4.2 Angular Correlation Procedure:

All the sources used during the angular correlation measurements were prepared by neutron irradiation of 2 mg of .008" iridium wire in the high flux positions of the McMaster reactor. Since the source material was natural iridium, the irradiation produced both 17 hour Ir^{194} and 74 day Ir^{192} activity in the ratio of about 25 to 1. For the Pt^{192} investigation the irradiation times were approximately 1-1/2 hours and the measurements were not begun until one week after the activation. This one week delay was sufficient to allow the Ir^{194} activity to decay to an insignificant amount. To produce the Ir^{194} activity necessary for the Pt^{194} experiments a 4 minute activation was performed.

Following the irradiation the wire source was placed in a thin quartz tube and mounted on a lucite pedestal which was attached to the micrometer table. The NaI detectors were positioned 7 cm. from the source while the semiconductor detector was some 2 cm. closer. The single channel analyzer (SCA) used to stabilize the high voltage supplies were set to select the 300 keV group. Once the NaI channels had been stabilized, the six SCA's were set to select the γ-rays of interest. All SCA's were originally set, and then periodically checked during a run, by means of a 512 channel pulse height analyzer. The source was centered with respect to the two moveable NaI detectors to within ±1/4% by monitoring the output

of one SCA in each NaI channel as a function of angle.

The programmer was set to perform an angle change every 45 minutes. Of this time, approximately 22 minutes were spent counting chance events, another 22 minutes counting true+ chance events, and about 1 minute monitoring the six singles rates. In the case of Pt^{192} the angular correlation measurements were carried out using two sources over a period of some six months, while the Pt^{194} measurements required eleven sources and about three months to complete.

A Fortran program to analyze the data typed out by the programmer was written and executed on a CDC 6400 computer. The program first performs a least squares fit to the singles rates to establish the original amount of short lived Ir^{194} and long lived Ir^{192} activity in each window. All the data are then corrected back to the time at which the experiment was begun. A statistical analysis of this corrected data is performed. The program establishes a mean value and standard deviation for each set of coincidences, four chance and four true+chance, and each set of singles rates. Any values which differ from the mean by more than 20 standard deviations are rejected. In this way spurious data, which might arise, for example, during card punching, is not included in the final analysis. Any remaining variation with angle in the singles rates is assumed to be the result of the source being off center, and the coincidence totals, true and chance, for each

angle are corrected accordingly. These corrected tables are fitted by the method of least squares to an even order cosine series:

$$W(\theta) = 1 + b_2 \cos 2\theta + b_4 \cos 4\theta$$

The coefficients b_2 and b_4 and the associated errors are the final result of the program.

From these values of b_2 and b_4 the coefficients of the even order Legendre polynomial series A_{22} and A_{44} (section 2.1) can be derived. The experimental coefficients are first corrected for the finite size of the detectors. Each coefficient must be multiplied by an attenuation factor, which is a function of the solid angle subtended by the detector and the energy of the γ-rays. Once this correction has been performed, the two sets of coefficients are related by the expressions of section 2.2.

4.3 Perturbed Angular Correlation Procedure

The sources for the perturbed angular correlation measurements were 1 mm. diameter, 3mm. long cylinders of iron containing 1 atom percent of natural iridium. To produce 100 μC of Ir^{194} activity these samples were neutron irradiated for approximately 10 minutes. For the Pt^{192} experiments this activation time was lengthened to about four hours, and, as in the angular correlation experiments, the counting was

not begun until one week after the irradiation. Each source was annealed for one hour at 1200°C to remove any radiation damage.

The alloy source was placed between the pole tips of an electromagnet mounted on the micrometer table. The distance from the source to the detectors, the stabilization windows and the six SCA's which selected the γ-rays of interest were left exactly as they were for the unperturbed measurements. The NaI detectors were positioned at the angles for which the slope of the particular angular correlation being rotated was largest. The power supply was adjusted to provide a magnet current of 1.5 A. For this coil current the magnetic field generated was about twice that required to saturate the sample.

The programmer was set up to execute the iron magnet cycle. The magnetic field direction was reversed every 10 seconds. The four coincidence totals were printed out every 45 minutes. One out of every four 45 minute cycles was spent counting chance coincidences. The six singles rates were monitored for about 40 seconds following each coincidence printout. Any fluctuations in these singles rates, other than that due to the decay of the source, were attributed to changes in the baselines or widths of the SCA windows. If one of these fluctuations was significant, the coincidence data for that 45 minute cycle was rejected. As during an

angular correlation run these windows were checked periodically and adjusted when necessary.

Since the half lives involved in all experiments were long compared to the switching time, no decay corrections were necessary. For each level studied the value of R (section 2.2) could be determined directly from the coincidence totals in the manner described in section 3.2.

To check the apparatus for the presence of systematic errors a measurement of R was made for a pure metal source. The value of R obtained using this diamagnetic source did not differ significantly from zero. Systematic errors can be the result of a stray magnetic field acting on the photomultiplier tubes, the detection of β particles, or a difference in the time for which the magnetic field is in one direction as opposed to the opposite direction. That diamagnetic R was zero implied that such errors had been eliminated.

4.4 Pt^{192} Experiments

A partial decay scheme for 74 day Ir^{192} is presented in Figure 3. The decay of this nucleus populates the high spin states of both Pt^{192} and Os^{192} as shown. The numbers in brackets above each transition indicate the branching ratios in percent. In a spectrum produced by a scintillation counter, the major γ-rays fall into three groups at 300, 468 and 600 keV. The 300 and 600 keV groups are in fact made up of three γ-rays each. This is evident in Figure 4 in which a spectrum

Figure 3: Partial decay scheme for Ir^{192} . The numbers in parentheses above each γ-ray are branching ratios in percent.

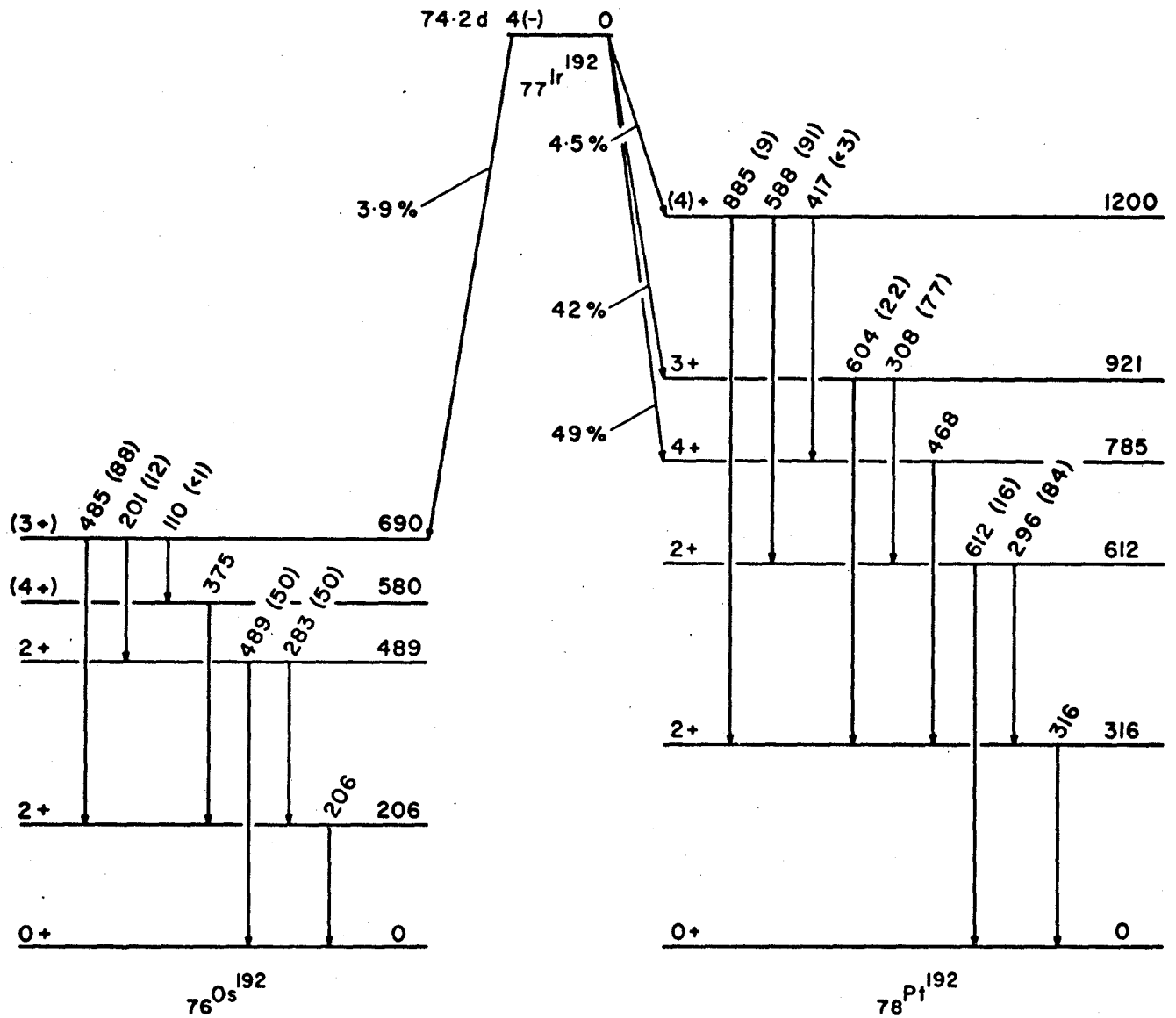
74·2d 4(-) 0
77Ir192
3·9%
4·5%
42%
49%
(4)+ 885 (9) 588 (91) 417 (<3) 1200
3+ 604 (22) 308 (77) 921
4+ 468 785
2+ 612 (16) 296 (84) 612
2+ 316 316
0+ 0
(3+) 485 (88) 201 (12) 110 (<1) 690
(4+) 375 580
2+ 489 (50) 283 (50) 489
2+ 206 206
0+ 0
76Os192
78Pt192

Figure 4: Singles spectrum of Ir^{192} observed with a Ge(Li) detector. The resolution is approximately 3 keV at 300 keV.

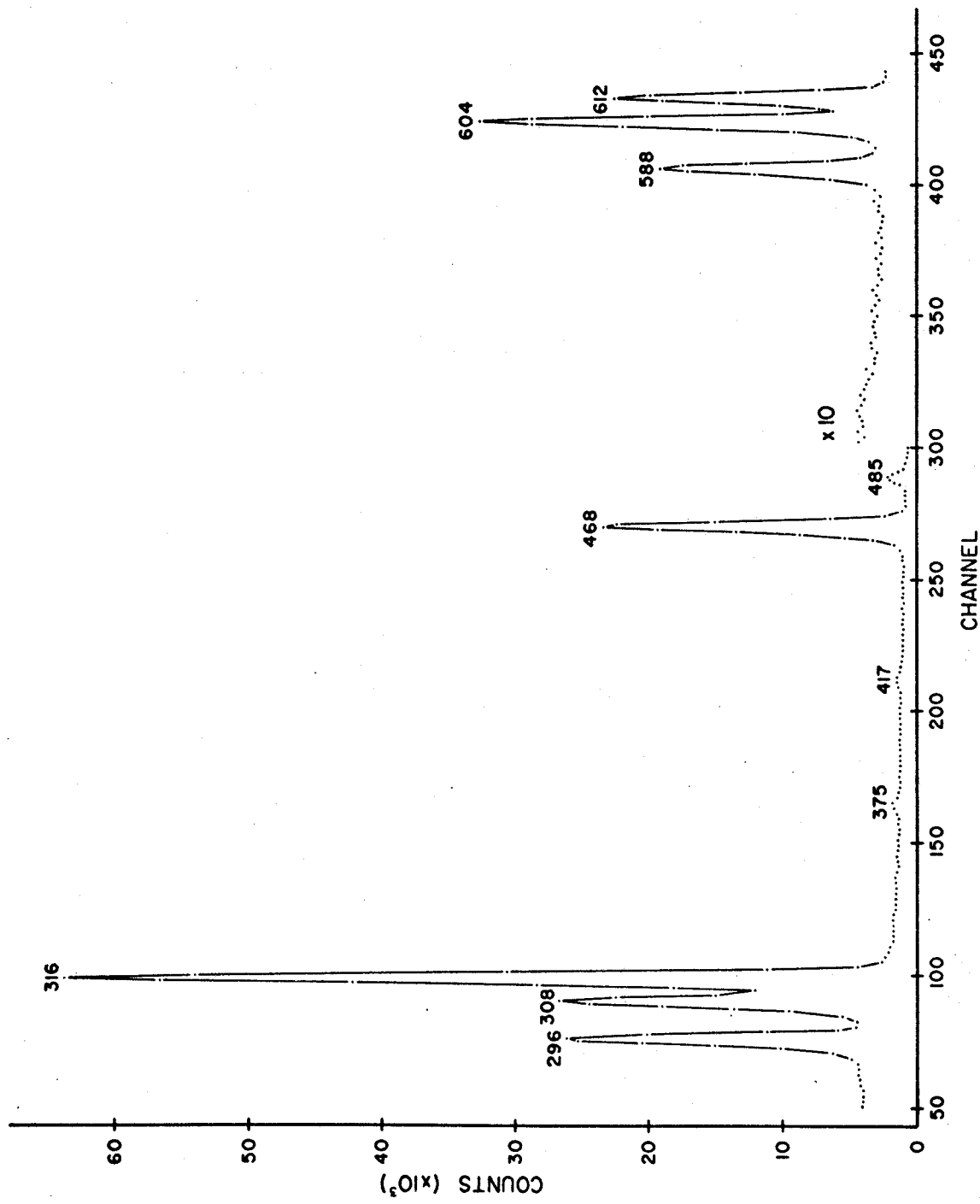
COUNTS (x10³)
0
10
20
30
40
50
60
CHANNEL
50
100
150
200
250
300
350
400
450
316
308
296
375
417
468
485
x 10
588
604
612

produced by the Ge(Li) detector is shown. The energies of the more prominent peaks are labelled, and two of these, the 375 and the 485 keV lines, are a result of transitions in Os^{192}.

The 316 keV level was studied using the 468-316 keV and the 604-316 keV cascades. The 612 keV level is the intermediate state in two strong cascades,588-296 and 308-612 keV. Since the former has an almost isotropic angular correlation function, the latter was chosen. In each of these three measurements, the SCA's in the Ge(Li) channel selected the lower energy peak while those in the NaI channels selected the higher energy group. The 300 keV region of the Ge(Li) singles spectrum is shown in Figure 5. The brackets indicate the windows used and the dashed curve represents the 316 keV peak intensity observed in coincidence with the 600 keV group. During these experiments, two of the three cascades were always being measured simultaneously.

A somewhat different procedure was used in the study of the 785 keV level. In this case separate windows were set on both the 417 keV and 468 keV peaks in the Ge(Li) spectrum. The four windows in the NaI channels were set to accept a band of pulse heights corresponding to an energy range of 400 to 480 keV. Figure 6 shows the relevant parts of the Ge(Li) singles spectrum.

The results of the angular correlation measurements

Figure 5: 300 keV region of Ge(Li) spectrum of Ir^{192}. The dashed curve indicates the 316 keV peak intensity observed in coincidence with the 600 keV group. The brackets show the range of pulse heights accepted by the single channel analyzers.

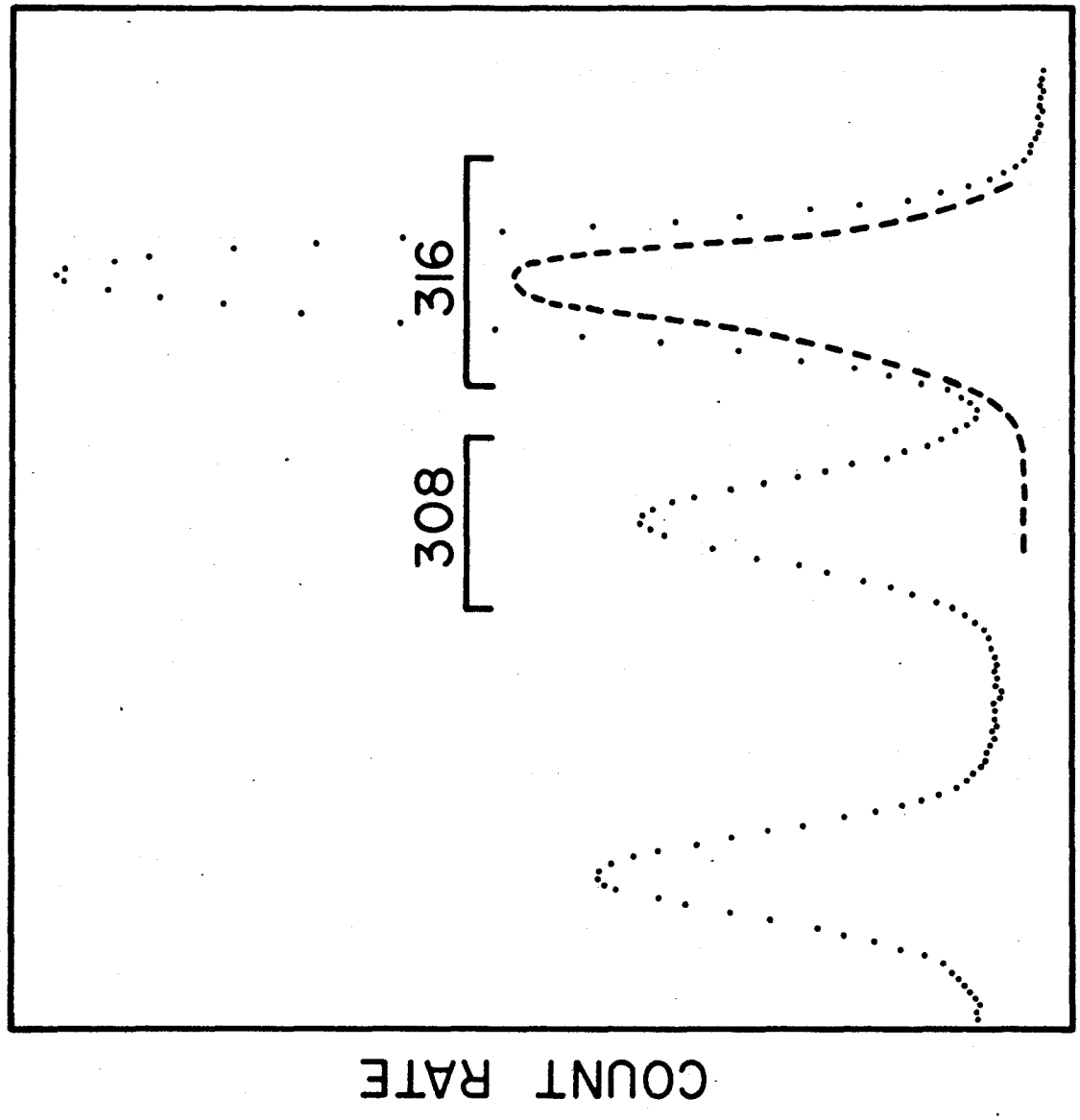
316
308
CHANNEL
COUNT RATE

Figure 6: 400 keV region of Ge(Li) spectrom of Ir^{192}. The expanded insert shows details of the 417 keV peak with underlying Compton edges from the 600 keV group.

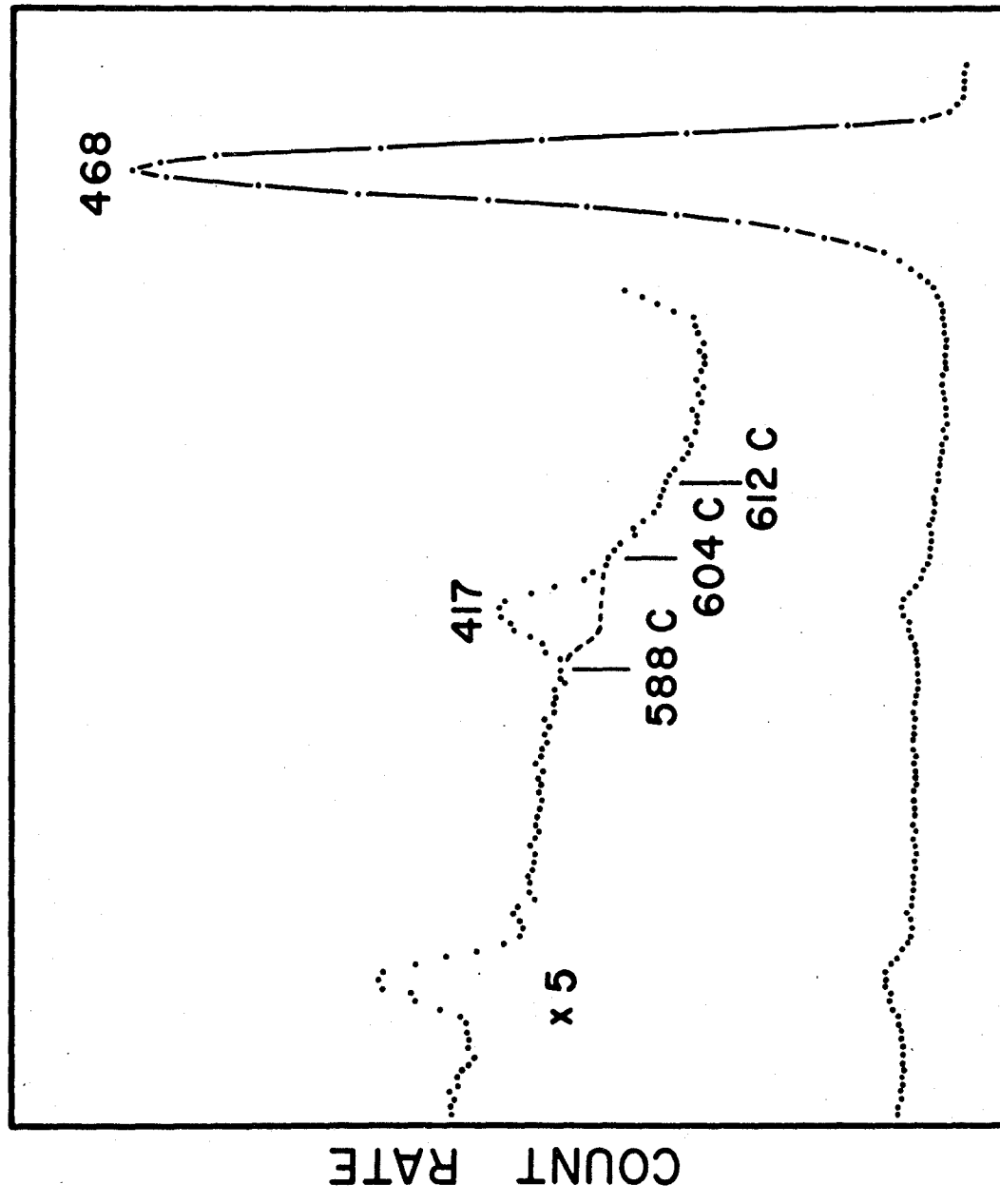
468
417
588 C
604 C
612 C
x 5
COUNT RATE
ENERGY

are summarized in Table I.

TABLE I

Angular correlation coefficients in Pt^{192}

Cascade	Spin Sequence	Experiment b_2	Experiment b_4	Corrected A_{22}	Corrected A_{44}
468-316 keV	4-2-0	0.050(2)	0.003(2)	0.100(8)	0.011(8)
604-316 keV	3-2-0	-0.204(5)	-0.011(5)	-0.410(15)	-0.070(22)
308-612 keV	3-2-0	-0.087(7)	-0.012(7)	-0.120(20)	-0.027(20)
417-468 keV	4-4-2	-0.059(19)	0.048(16)	-0.120(26)	0.110(30)

The final column contains the coefficients of the Legendre polynomial series for $W(\theta)$. These coefficients have been corrected for the finite size of the detectors, and for competing cascades. The 468-316 keV cascade contains a contribution of about 8% from the highly anisotropic 604-316 keV cascade. This arises as a result of 604 Compton events being accepted by the 468 keV window in the NaI channel. In the case of the 604-316 keV cascade, there is an isotropic background contribution of about 36%. This is due to 588-(296)-316 keV events and 308-296 keV sum events which appear in the 600 keV window in the NaI channel. The 308-612 keV cascade contains a part of the 604-316 keV cascade since the 308 keV window will accept some 316 events (see Figure 5). This latter contribution is of considerable importance since it affects the g factor measurements. The spectral line shape in the Ge(Li) detector was established using a Cr^{51} source. This source produces a

clean line at 320 keV. Care was taken to ensure that the count rate was the same as that in the iridium decay measurements. In this way, the contribution to the 308 keV peak from the 316 keV γ-ray was found to be 13±2% in the singles spectrum and 7±2% in coincidence with the 600 keV group.

Since the magnetic measurements were performed under the same conditions of geometry and count rate as the angular correlations, the experimental angular correlation coefficients b_2 and b_4 were used to calculate the slopes required in the analysis. The one exception to this procedure was the 308-612 keV cascade, 7% of which was found to be made up of 604-316 keV coincidences. This latter cascade passes through the 316 keV level, and hence the precession of this level must be taken into account when evaluating that of the 612 keV level. The results of the magnetic measurements are shown in Table II.

TABLE II

Results of magnetic measurements for Pt^{192}

Level	ωτ(rad.)	τ(ps)	g
316 keV	0.088(5)	51(4)	0.34(5)
612 keV	0.047(11)	29(3)	0.30(8)
785 keV	0.014(10)	17(3)	0.14(11)

The g factors have been derived using the hyperfine field at platinum nuclei in iron measured by Kontani and Itoh, 1967. Corrected to room temperature the value of this field is

1250±39 k0e. The mean lives shown in the table were measured by Schwartzschild, 1966 (316 and 785 keV levels) and Beraud et al, 1969 (612 keV level).

4.5 Pt^{194} Experiments

Figure 7 contains a partial decay scheme for 17 hour Ir^{194}. The spin of this nucleus is 1- and hence its decay does not tend to populate the high spin states of Pt^{194} as was the case in the decay of Ir^{192} to Pt^{192}. As a result, 89% of the decays are to the ground state, and in fact, only 2% of them populate the initial state of the two cascades studied. When the specific activity of the source was high enough to produce a usable γ-ray count rate, the flux of high energy β particles was considerably higher than in the Pt^{192} experiments. Care was taken to ensure that these β particles were not being detected.

A singles spectrum for the energy range of interest produced by the Ge(Li) detector is shown in Figure 8. The peaks marked with an "x" are the result of transitions in Pt^{192}. The 939-329 keV cascade was used in the study of the first 2+ level, while the 645-622 keV cascade was selected for the measurements involving the second 2+ state. Both of these cascades involve E2 transitions through an 0-2-0 spin sequence and hence the angular correlation patterns are very anisotropic. The SCA's in the Ge(Li) channel were set to

Figure 7: Partial decay scheme for Ir^{194}. The numbers in parentheses above each γ-ray are branching ratios in percent.

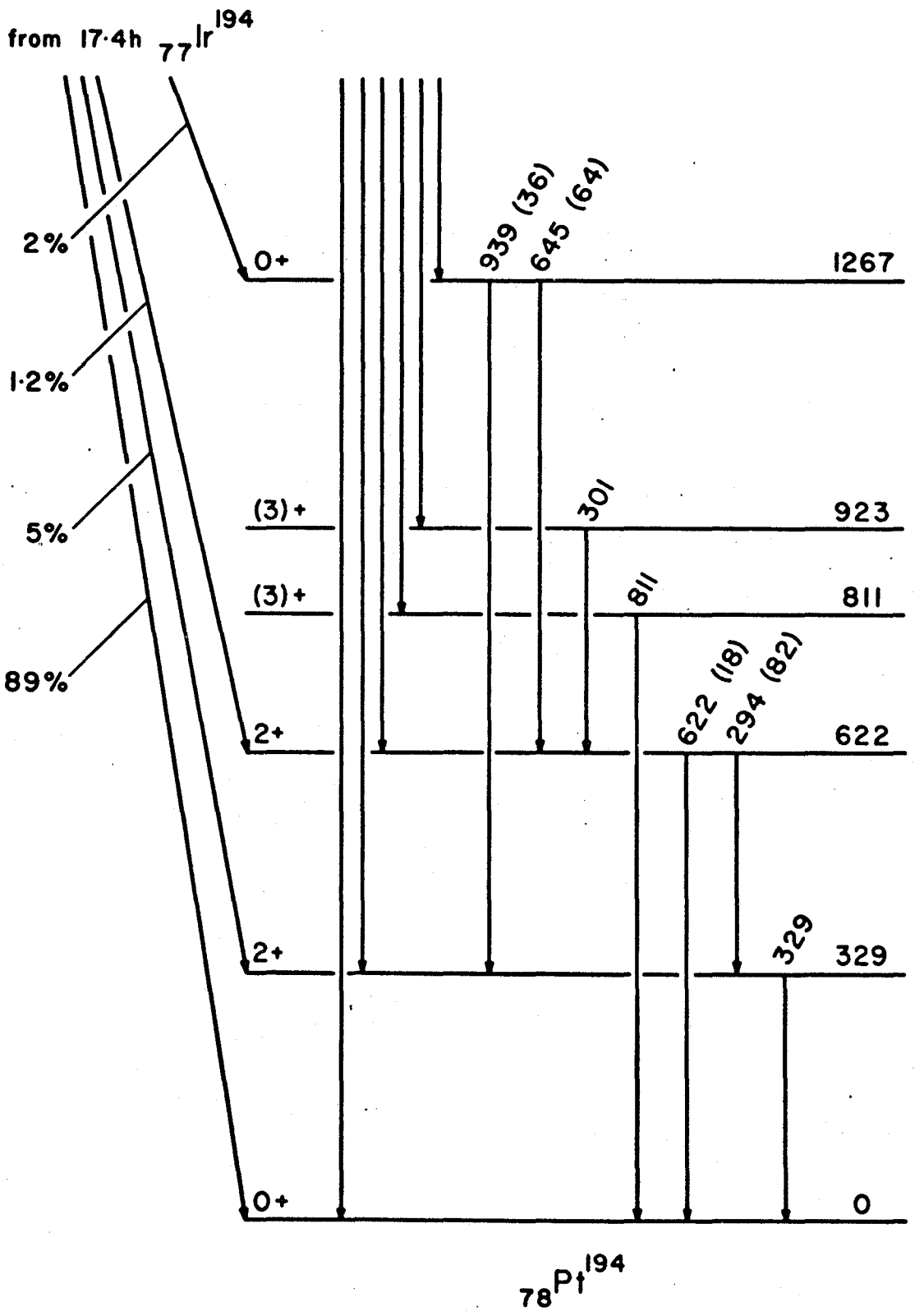
from 17·4h $_{77}Ir^{194}$
2%
1·2%
5%
89%
0+
(3)+
(3)+
2+
2+
0+
939 (36)
645 (64)
301
811
622 (18)
294 (82)
329
1267
923
811
622
329
0
$_{78}Pt^{194}$

Figure 8: Ge(Li) spectrum of Iridium approximately 12 hours after neutron activation. The resolution is 3 keV at 300 keV.

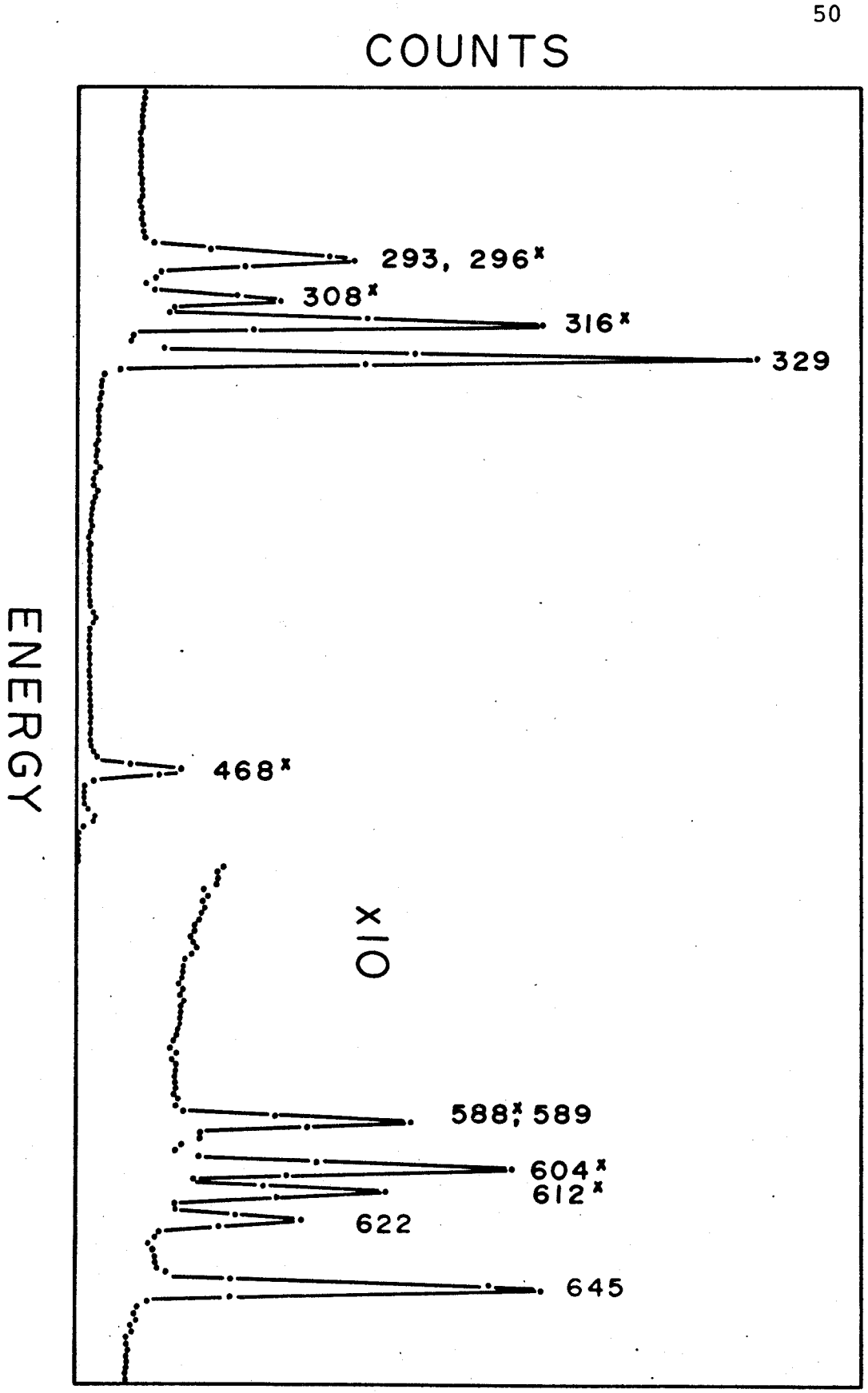
COUNTS
ENERGY
293, 296x
308x
316x
329
468x
x10
588x, 589
604x
612x
622
645

select the lower energy γ-rays of each cascade, while the two scintillation counters were used to observe 939 and 622 keV events.

The angular correlation coefficients b_2 and b_4 measured for the two cascades are presented in Table III.

TABLE III

Angular correlation coefficients in Pt^{194}

Cascade	Experiment		Theory	
	b_2	b_4	b_2	b_4
939-329 keV	0.18(1)	0.24(1)	0.40	0.35
645-622 keV	0.18(4)	0.19(4)	0.40	0.35

The theoretical angular correlation coefficients shown in the table have been corrected for attenuation due to the solid angles subtended by the counters. The discrepancy between these theoretical values and the experimentally determined ones is a result of backgrounds present in the windows. The germanium counter spectrum in coincidence with the 900 keV window contains only 1 or 2% background in the 329 keV peak region. This is shown in Figure 9(a). However, the 900 keV window in the scintillation spectrum contains approximately a 50% contamination from higher energy Compton events. Figure 9(b) is part of a Ge(Li) spectrum in coincidence with 600 keV events in the scintillation counter. As the figure

Figure 9: Coincidence spectra of Ir^{194}

(a) Part of the spectrum in coincidence with the 939 keV γ-ray selected in a scintillation counter.

(b) Part of the spectrum in coincidence with 600 keV.

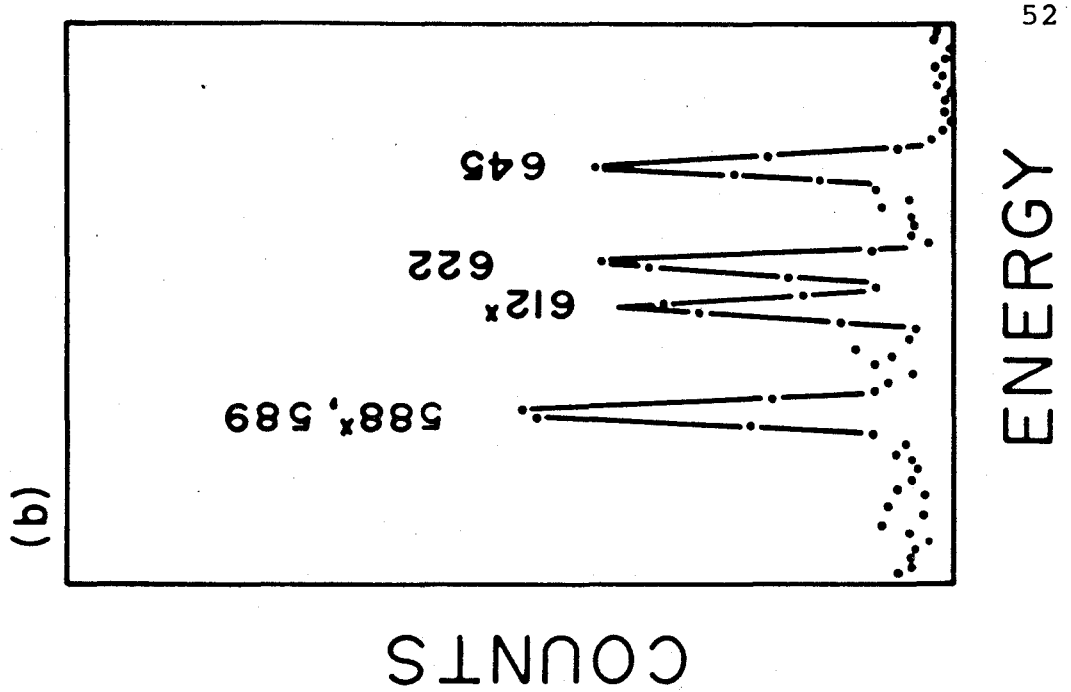
(a)
COUNTS
ENERGY
329
316*
293, 296*

(b)
COUNTS
ENERGY
588*, 589
612*
622
645

shows, the Ge(Li) window selects the 645 γ-ray clearly. The background in the area of this peak is once again only 1 or 2% and certainly not large enough to account for the 50% reduction in the coefficients b_2 and b_4. The detection of the 622 keV γ-ray in the scintillation counter however is complicated by the presence of 293-329 sum events. For the count rates involved in these experiments, these sum events accounted for about 30% of the 600 keV peak intensity. The angular correlation coefficients for the 645-(293+329) keV triple coincidence are large and negative. This is the reason that the experimental coefficients are smaller than predicted.

For both levels the perturbed angular correlation may be correctly interpreted using the experimental coefficients b_2 and b_4. In the case of the 329 keV level, the contamination was due to Compton events as discussed earlier. The majority of the high energy γ-rays stop at either the ground state or the 329 keV state. The competing cascade present in the study of the second excited state is the 645-(293+329) keV triple coincidence. In this case, the rotation of the 329 keV level does not enter into the evaluation of $\omega\tau$ for the 622 keV state since the 293-329 coincidences are always detected at 0°. This is a local extremum of the angular correlation pattern, and so, while both levels are being rotated, only the rotation of the 622 keV level is observed. The results of the magnetic measurements are contained in Table IV.

Figure 10: The angular distribution function for the 939-329 keV cascade in Pt^{194}. The curve is a result of a least squares fit and corresponds to the coefficients shown.

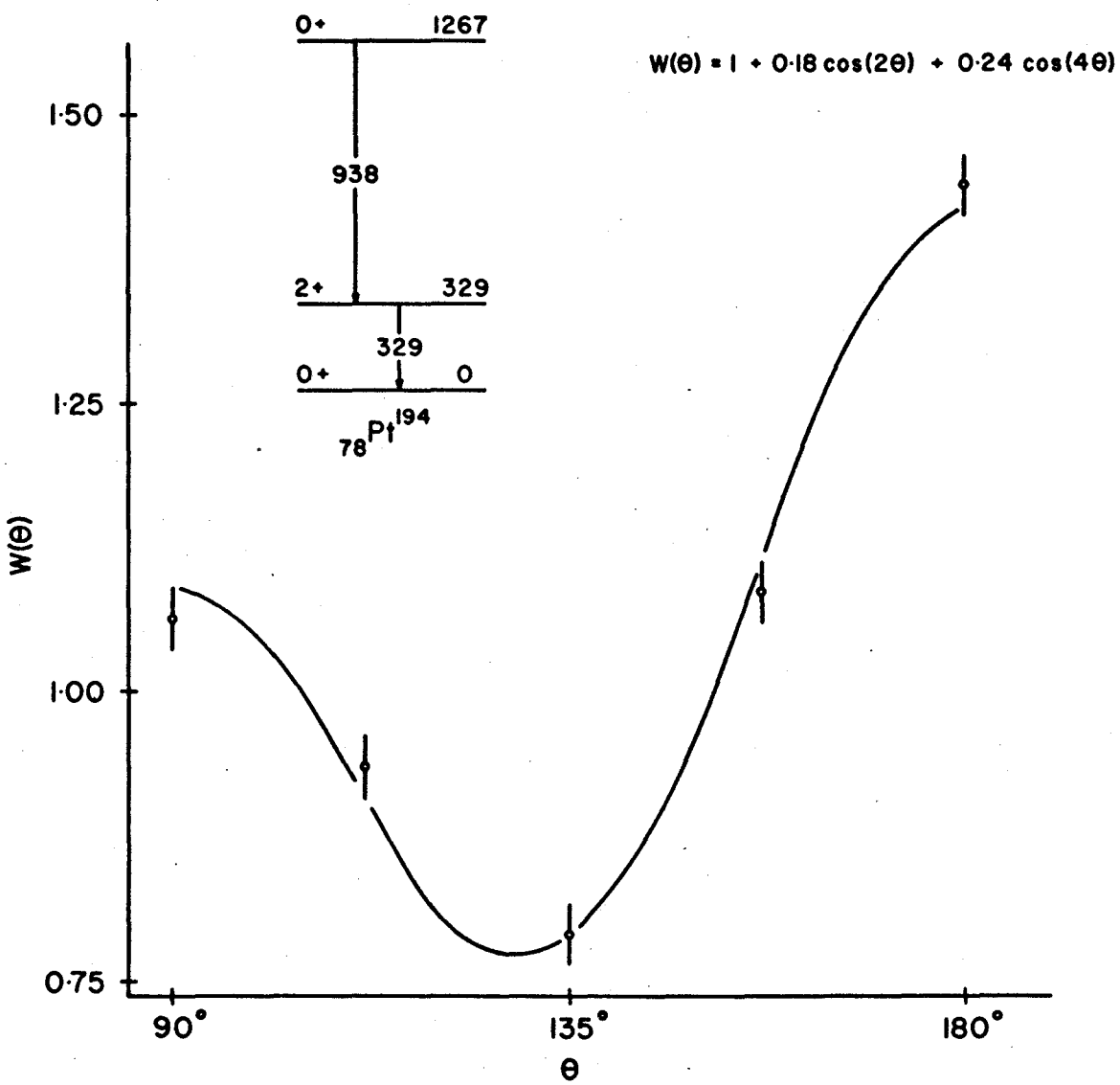
0+ 1267
938
2+ 329
329
0+ 0
78Pt194
W(θ) = 1 + 0·18 cos(2θ) + 0·24 cos(4θ)
1·50
1·25
1·00
0·75
W(θ)
90°
135°
180°
θ

TABLE IV

Results of magnetic measurements for Pt^{194}

Level	R	$\omega\tau$ (rad)	τ (ps)	g
329 keV	0.185(5)	0.087(4)	53(6)	0.27(3)
622 keV	0.167(14)	0.091(15)	63(9)	0.24(5)

The mean lifetimes of the states have been measured by Bruton et al, 1969. They were derived from Coulomb excitation cross sections for these levels. Using these lifetimes and a value of 1250±30 k0e for the hyperfine field (Kontani and Itoh, 1967) the two g factors were obtained.

CHAPTER V

DISCUSSION

5.1 Introduction

The tungsten, osmium, and platinum nuclei lie in a region of transition, a region of onset or disappearance of nuclear deformation, and provide a crucial testing ground for nuclear structure models. The Bohr Mottelson idea of collective quadrupole motion, that is the cooperative movement (λ=2) of many nucleons, appears to be valid for the low lying levels of such nuclei. This is evidenced by the B (E2, 0→2) values which are 60-100 single-particle units and by the smooth variation with A of the properties of these levels. However the energy levels and electromagnetic moments of these transition nuclei show large deviations from both the rotational model and the phonon model. Attempts to understand these deviations in terms of small corrections (for example, band mixing) to the rotational model have not been very satisfactory.

In this chapter the experimental results of this and other investigations of the Pt nuclei are compared with the predictions of a model developed by Kumar and Baranger. The basic assumptions, formalism, and predictions of this model are contained in a series of papers published between 1965 and 1968 (Kumar and Baranger, 1966 and 1968; Baranger and

Kumar, 1965 and 1968).

5.2 Pairing-Plus-Quadrupole Model

The "true" residual force in nuclei is presumably quite different from a pairing-plus-quadrupole (P+Q) force. Nevertheless, it is a popular microscopic description of the nucleus, since the "true" force does lead to pairing and deformation, and calculations with a P+Q force are relatively simple.

The Hamiltonian of the model consists of three parts:

$$H = H_s + H_p + H_q$$

The first part is the spherical, single-particle energy. In second-quantized notation it is:

$$H_s = \sum_\alpha \varepsilon_\alpha \, C_\alpha^+ \, C_\alpha$$

where α denotes all quantum numbers necessary to specify a state.

$$\alpha \equiv (n, \ell, j, m)$$

The wave functions are those of an isotropic harmonic oscillator. The parameters ε_α, which do not depend on the magnetic quantum number m, give the sequence of single-particle levels in spherical nuclei.

The second part of the Hamiltonian is a pairing force of strength g:

$$H_p = -\frac{1}{4} g \sum_{\alpha\gamma} S_\alpha \, S_\gamma \, C_{\bar{\alpha}}^+ \, C_{\bar{\gamma}} \, C_\gamma$$

where $\bar{\alpha} \equiv (n, \ell, j, \bar{m})$ and $S_\alpha = (-1)^{j-m}$

The third part of M is a quadrupole force of strength ψ:

$$H_q = -\frac{1}{2} \psi \sum_{\alpha\beta\gamma\delta} \sum_m \langle \alpha | Q_m | \gamma \rangle \langle \delta | Q_m | \beta \rangle \, C_\alpha^+ \, C_\beta^+ \, C_\delta \, C_\gamma$$

The operator Q_m is the quadrupole moment $Q_m = r^2 Y_{2m}(\theta,\phi)$ and M takes the values -2, -1, 0, 1, 2. The quadrupole force between two particles is just the tensor product of the quadrupole moment times $-\psi$.

5.3 Deformation and the Pairing-Plus-Quadrupole Model:

In the calculations of Kumar and Baranger this microscopic description of the nucleus, the pairing-plus-quadrupole model, is used to calculate Bohr's collective Hamiltonian. This collective Hamiltonian contains seven arbitrary functions of β and γ; the potential energy, the three moments of inertia, and the three vibrational inertial parameters.

$$H_{Bohr} = V + T_{rot} + T_{vib}$$

$$V = V(\beta,\gamma)$$

$$T_{rot} = \sum_{i=1}^{3} \frac{1}{2} \phi(\beta,\gamma)\, Wi^2$$

$$T_{vib} = \frac{1}{2} B_1(\beta,\gamma)\dot{\beta}^2 + B_2(\beta,\gamma)\dot{\beta}\dot{\gamma} + \frac{1}{2} B_3(\beta,\gamma)\dot{\gamma}^2$$

These seven functions are calculated by applying time dependent Hartree-Bogolyubov techniques to the pairing-plus-quadrupole model. The Hartree-Bogolyubov method is simply an extension of the Hartree-Fock method which includes pairing.

Two experimental facts are used to simplify the calculation. One is that nuclear deformations are mostly of a quadrupole nature. This theory retains the collective model approximation of pure, quadrupole motion, uncoupled to the higher-lying modes like pairing vibrations, octupole modes; and single-particle

excitations. The other is that for heavy nuclei actual nuclear shapes are only small modifications of the spherical shape, that is β is not very large. This theory is restricted to $\beta<0.3$.

The theory treats all nuclei on the same basis and a priori assumptions about the nuclear shape are not necessary. The phonon and rototional models represent the two limits of quadrupole motion and deviations from these two limits are treated in a natural way. The usual approximation of harmonic vibration either about a spherical or a deformed shape is not made. The anharmonicity of quadrupole motion is determined by the seven functions of Bohr's collective Hamiltonian. The anharmonic terms cause band mixing in deformed nuclei and phonon mixing spherical nuclei.

The input to this calculation consists of a set of spherical single-particle levels, the strength of the proton and neutron pairing forces, the strength of the quadrupole force ψ, and an inertial constant representing the core contribution.

Ideally the sets of single-particle levels used should be varied to obtain the best overall fit. However, to render the calculation practical, the set of levels first used by Mottelson and Nilsson (1959) were used throughout. The maximum number of levels used in the calculations is two major oscillator shells. The two shells used for neutrons and for protons are not necessarily the same. Matrix

elements of the quadrupole force involving the upper one (mostly unfilled) of the two adjacent shells tend to be too large compared to those involving only the lower shell. The influence of the upper shell is decreased by multiplying all quadrupole matrix elements between states of the upper harmonic oscillator shell by a factor K:

$$K = (N + 3/2) \; / \; (N + 5/2)$$

where N is the total quantum number of the lower shell. This somewhat arbitrary attenuation factor was obtained from a comparison of the quadrupole force with several "realistic" forces.

The pairing strengths used are:

$$Gp = 27 \text{ Mev} \; / \; A$$

$$Gn = 22 \text{ Mev} \; / \; A$$

These strengths were determined by fitting odd-even mass differences in deformed nuclei. As usual, the assumption of no neutron-proton pairing is mode. This is justified on the ground that for heavy nuclei the neutrons and protons are filling different oscillator shells and hence their wave-functions have little overlap.

The strength of the quadrupole force ψ was determined by fitting experimental quadrupole moments. The n-n, n-p and p-p quadrupole forces were assumed to be equal. These fits were made for the entire region of Z =50-82 and N=83-126 rather than for each individual nucleus.

It is not a good approximation to use a quadrupole

force for interaction between core nucleons and external nucleons. In this theory, the core is represented by a harmonic oscillator which is coupled to the external nucleons by a quadrupole force. The constant describing this core was established by fitting the experimental moments of inertia over the range Z=50-82 and N=82-126.

Energy levels, transition probabilities, and static moments are calculated by using a completely numerical method for solving Bohr's Hamiltonian. In this method, no assumptions are made about the separation of rotation, β motion, or γ motion; coupling between the three kinds of motion is treated exactly. This coupling is determined by the seven functions of the Hamiltonian which are calculated at each point of a $\beta - \gamma$ mesh. The Schrodinger equation is solved by the variational method, the variational parameters being the values of the wave function at all points of the mesh.

5.4 Results of the Calculations

Calculations have been performed by Kumar and Baranger (1968) for the lowest two 0+, three 2+, one 3+, and one 4+ states of the tungsten, osmium and platinum nuclei. The main results are presented in this section.

One result of these calculations was that the lowest potential minimum corresponds to a deformed, prolate shape for $W^{182-186}$ and $Os^{186-188}$; an asymmetric shape for $Os^{190-192}$

(the hole is only 100 KeV deep); and an oblate shape for $Pt^{192-196}$. The ground-state wave function does not show such a marked transition since the potential minimum becomes shallower at large A and the wave function is smeared over all possible shapes. It does not look at all like a Gaussian centered at the origin as the phonon model requires.

The calculations for the Pt isotopes provide a simple explanation for the spectroscopic quadrupole moments of these near spherical nuclei. The calculated moment of the first 2+ states is positive, which corresponds to an oblate intrinsic shape, and increases rapidly from 8% to 68% of the rotational value in going from Pt^{192} to Pt^{196}. These large quadrupole moments are a result of the nucleus vibrating about a deformed shape. However the energy levels follow the phonon model pattern approximately because the deformed minimum is shallow and the nucleus has enough zero-point energy (even in the ground-state) to go over the spherical barrier. Table V contains the calculated and experimental quadrupole moments for the first 2+ states of the Pt nuclei.

TABLE V

Static quadrupole moments of Pt nuclei

A	Q2+	Q2+ / Q2+ R.M.	Q2+ Exp.
192	0.092	0.08	-
194	0.492	0.39	0.84 (16)
196	0.699	0.68	0.56 (21)
198	-	-	1.22 (50)

A comparison with those values predicted by the rotational model is made in column three, while column four contains the experimental values of Glenn and Saladin (1968). The agreement while not spectacular, is reasonable and certainly better than that obtained with either the phonon model or the rotational model.

The results of all the perturbed angular correlation measurements made on Pt^{192} and Pt^{194} are collected in Table VI.

TABLE VI

Larmor precession of levels of Pt nuclei

A	Level	WT (red)	
192	316 KeV	0.068 (7)	Cameron (1964)
		0.092 (8)	Buyrn and Grodzins (1964)
		0.063 (9)	Keszthelyi et al (1965)
		0.080 (5)	Agarwal et al (1966)
		0.067 (6)	Murray (1967)
		0.070 (5)	Grabowski (1969)
		0.088 (5)	This work
		0.076 (3)	Weighted average
192	612 KeV	0.040 (10)	Grabowski (1969)
		0.047 (11)	This work
		0.043 (7)	Weighted average
192	785 KeV	0.014 (10)	This work
194	329 KeV	0.092 (7)	Keszthelyi et al (1965)
		0.099 (9)	Agarwal et al (1966)
		0.087 (4)	This work
		0.089 (3)	Weighted average

Table VI cont.

194	622 KeV	0.079 (15)	Keszthelyi et al (1965)
		0.083 (20)	Agarwal et al (1966)
		0.091 (15)	This work
		0.084 (9)	Weighted average

Table VII contains experimental values for B (E2) and g factors for Pt ^{192} and Pt ^{194}. The predictions of Kumar and Baranger (1968) are also presented.

TABLE VII

Electromagnetic properties of Pt nuclei

A	Level	B(E2) Exp.	B(E2) Theory	g Exp	g Theory
192	316 KeV	2.54 (25)	1.81	0.30 (3)	0.22
192	612 KeV	0.023 (4)	0.005	0.28 (7)	0.22
192	785 KeV	-	-	0.14 (10)	0.21
194	329 KeV	1.94 (20)	1.70	0.28 (3)	0.22
194	622 KeV	0.011 (2)	0.005	0.22 (4)	0.22

The experimental values for the B (E2) are those of Bruton et al (1969) and the experimental g factors have been calculated using the weighted averages of Table VI.

Table VIII presents a comparison of experimental and theoretical mixing ratios in Pt ^{192}.

TABLE VIII

γ-ray mixing ratios in Pt^{192}

Transition	308	604	
δ_{Exp}	-9.4 (15)	3 (1)	This Work
	-9.9 (10)	2.0 (2)	Grabowski (1969)
	-7.3 (10)	2.1 (3)	Hamilton and Davies (1968)
δ_{Theory}	-9.1	2.4	Kumar and Baranger (1968)

As can be seen from inspection of these last two tables, the agreement between experimental values and those predicted by Kumar and Baranger is quite good. Their calculations give the correct order of reduction of the g factors from the hydrodynamic value of Z/A (0.4 for this mass region.)

CHAPTER VI

CONCLUSION

The method of perturbed angular correlations has added significantly to the available data on magnetic moments of excited nuclear states. However, very few levels remain which can be studied by the method of this investigation. It is no longer feasible to perform an original measurement using scintillation detectors and a source produced by neutron irradiation. Some worthwhile re-measurements can still be performed using high resolution Ge(Li) detectors with this type of source. However, a more useful approach is to populate a new set of levels by means of coulomb excitation, (p,n) or (α,n) reactions, and attempt to observe the Larmor precession of these levels.

In general, any level that can be populated by coulomb excitation, (p,n) or (α,n) reactions can be studied by the method of perturbed angular correlations provided that level satisfies the following three conditions: (a) the lifetime of the level must be of the order of 100 picoseconds, (b) the de-excitation γ-ray must have a non-isotropic angular distribution, and (c) it must be possible to make a suitable alloy target. A suitable alloy is a ferromagnetic one with a high Curie temperature, well understood magnetic properties, and few competing reaction γ-rays.

There are a number of light nuclei which could satisfy these conditions. (p,n) and (α, n) reactions on iron, copper, cobalt, and manganese populate levels for which a rotation may be observed. In the case of these reactions, the angular distribution pattern of the γ-rays can be made more anisotropic by detecting the coincident neutrons at 0^0. Otherwise the incident beam energy should be adjusted to be near the reaction threshold, so that most of the neutrons will come off near 0^0.

One possible level is the 339 KeV state in Ni^{59}. This level can be populated by the (α, n) reaction on a natural iron target. The energy of the alpha beam need only be 10 MeV. The angular distribution of the de-excitation γ-ray has already been observed to be anisotropic. Since the target would be natural iron there would be no alloy to be produced and hence no impurity γ-rays to clutter up the Ge(Li) spectrum. Another possibility is the 112 KeV state in Co^{58} which is populated by the (α,n) reaction on manganese. In this case the target could not be the pure metal, but would have to be a ferromagnetic alloy. One possible alloy is MnSb: antimony is heavy enough that there would be no competing (α,n) reaction.

In principle, a great many new levels can be studied by this method of perturbed angular correlations, and the magnetic moments derived from these measurements could be used as a further check of nuclear models.

APPENDIX I

CARD 1: (see Figure 11)

This card generates five sets of timing pulses of various frequency, which are used by the logic on the remaining cards. The clock is a simple 20 bit scaler (FF-1 to FF-20) with a Schmidt trigger (N-1A, N-1B, and N-1C) on its input. The input to this trigger can be either 5 to 10 volt positive pulses or a 5 to 10 volt sine wave. The frequency of these pulses should not exceed 100cps. The clock is cleared via two power gates (B-1A and B-1B). The power gates are necessary because of the relatively high fan-out (20). A negative going pulse (+5v. to gnd.) at the input of B-1A sets all flip-flops to the "0" state. The "1" states of these flip-flops go off this card to five tap switches on the front panel, and five of them are returned to invertors I-1A to I-1E. These five square waves of various frequencies make up the inputs to five pulse shaping monos (1μs pulse width). Finally, these five pulse lines leave the card via the rear 22 pin connector, and are available to the other cards via the rear board. The clock is enabled by a +5 volt level on the gates of FF-1, and disabled by a gnd. level on these gates (the level on this enable line is controlled by FF-15 on Card 2.)

CARD 2: (see Figure 12)

This card contains the logic which controls an experiment. Three control cycles exist; iron magnet cycle (IM), superconducting magnet cycle (SCM), and angular correlation cycle (AC).

FF-1 to FF-3, M-1, N-1A and N-1B make up the IM control logic. To begin with, the three flip-flops are cleared via the CLEAR 2 and CLEAR 3 lines. When IM CYCLE IN-OUT switch is in the IN position, gate N-1B is open and allows IM CYCLE pulses to pass. The frequency of these pulses is typically 0.1 cps. The first of these pulses to get through this gate appears as a negative going pulse on the set terminal of FF-3. When FF-3 is set to the "1" state, gate N-1A opens and allows CYCLE pulses (typically 6 cps.) to pass. The first of these toggles FF-1 into the "1" state, thus shutting the coincidence gates, and toggling FF-2 into the "1" state. This change in state of FF-2 reverses the iron magnet field direction by means of a small DPDT relay. The second CYCLE pulse to pass through N-1A toggles FF-1 back into the "0" state, opening the coincidence gates; but FF-2 remains in the "1" state. As the "1" side of FF-1 falls to gnd., M-1 fires and clears FF-3. This shuts N-1A and completes a field reversal. The next IM CYCLE pulse

initiates another field switch in a similar manner (FF-2 is returned to the "0" state). Thus, for each IM CYCLE pulse, the coincidence gates are close, the field direction is reversed, and then the coincidence gates are re-opened.

Chance control consists of FF-4 to FF-7, N-1C, N-1D, N-2A, N-2B, N-7A, and N-7B. FF-4 to FF-7 make up a simple four bit scaler which counts the total number of cycles which have been completed. The outputs of gates N-2A, N-2B, N-7A and N-7B fall to gnd. only every other, third, seventh and fifteenth cycles respectively. One of these outputs is selected by a tap switch on the front panel, and then inverted by N-1D and sent via an emitter follower to the timing SCA's. When a +5 volt level appears on this line to the SCA's, a 500ns delay is inserted in the fast timing circuits. Hence, any coincidences recorded with this line a +5 volts must be chance events.

SCM control logic consists of FF-8 to FF-13, N-4A N-3A, N-6B, N-6C, and N-6D. A negative going pulse on the CLEAR 5 line sets a "1" in FF-8 and clears the other five flip-flops. N-3A is open, since FF-8 is in the "1" state and FF-10 is in the "0" state. The first CYCLE pulse to pass through this gate appears as a negative going pulse on the clock input of FF-8 and the set terminal of FF-10. FF-8 toggles into the "0" state, resulting in a change in

motor direction, and FF-10 is set to the "1" state. As the "1" side of FF-8 falls to gnd., FF-9 toggles into the "1" state, resulting in a change in the SCM field direction. Gate N-3A is now closed because of the status of both FF-8 and FF-10. Since FF-10 is now in the "1" state, gate N-4B is open, allowing the passage of MOTOR ON TIME pulses. The frequency of these pulses is selected by a front panel switch, and is typically 0.025 cps. The first of these pulses to pass through the gate toggles FF-11 into the "1" state, which turns on the motor. The second of these pulses returns FF-11 to the "0" state, which shuts off the motor. As FF-11 does so, FF-10 is toggled into the "0" state as well. This shuts N-4B and the motor cycle is complete. The field direction has been reversed via FF-9 and the motor has raised the magnet current up to its operating level. FF-12 and FF-13 play no part in this portion of the cycle. At the end of the cycle, an E of C pulse appears at the input of N-4A. This toggles FF-8 into the "1" state, reversing the motor direction, and sets FF-10 into the "1" state, opening gate N-4B. Note that N-3A is held shut at this time by FF-10. The motor is now prepared to drive down the magnet current, and does so when the first MOTOR ON TIME pulse passes through gate N-4B. When the second of these pulses returns FF-11 to the "0" state, shutting off the motor, FF-10 is toggled into the "0" state.

This closes N-4B and opens N-3A, and a CYCLE pulse passes through the latter gate. This pulse switches the motor direction via FF-8, and then the motor flip-flop (FF-11) runs through its cycle, as described above. FF-12 and FF-13 count the number of times that the motor has been turned off in any one cycle. When the motor has been turned off twice (as is the case when the magnet current has been returned to operating value) FF-13 opens the coincidence gates and counting begins. These two flip-flops are cleared at the end of each cycle, so that the coincidence gates are shut before the motor drives the magnet current down. Thus, at the end of each cycle (typically 45 minutes) the coincidence gates are closed, the SCM current is slowly reduced to zero, the field direction is reversed, the SCM current is slowly increased to a preset level, and then the coincidence gates are opened.

FF-15 and gates N-5A and N-5B are used to generate a level which either enables or disables the clock. FF-15 is cleared via the CLEAR 4 line and the clock is disabled. To start the clock, the START pushbutton is depressed. This sets FF-15 to the "1" state raising the enable line to +5 volts. To stop the clock FF-15 is cleared by means of the front panel pushbutton labelled PAUSE. Note that disabling the clock does not shut any of the gates on lines to the six

scalers, and they will continue to record events.

CARD 3: (see Figure 13)

This card contains input amplifiers and gates, and the logic which generates a read command at the end of a singles counting period.

The ten identical (except for small variations in resistor valves) amplifiers are simple invertors utilizing high frequency switching transistors (2N708). The inputs to these amplifiers are clamped to ground by diodes (1N913). A positive going, 10 volt pulse at the input results in a negative going (+5 volts to gnd.) pulse at the output. To ensure that these pulses go below gate thresholds (typically 1 volt), the emitters of all transistors are tied to -0.7 volts generated by a forward biased silicon diode (1N4005).

The outputs of amplifiers 1 to 4 are inverted by N-5A to N-5D and then gated by N-1A to N-1D. These gates are open only when the line labelled COINC GATES is high. The negative going pulses at the outputs of these gates are inverted and become inputs to gates N-3A to N-4D. The purpose of these gates is to switch the inputs to scalers 1 and 2, and scalers 3 and 4 each time the field direction is reversed. When the field direction is "down" (as it is when the machine

has just been reset) the line labelled S. UP is at +5 volts, and gates N-3A to N-3D are open. Thus conicidence inputs 1,2,3, and 4 are directed to scalers 1,2,3, and 4 respectively. When the field direction is reversed, the strobe line S.UP falls to gnd. and the other four gates N-4A to N-4D are open. This results in inputs 1,2,3, and 4 being directed to scalers 2,1,4, and 3 respectively.

The outputs of amplifiers 5 to 10 are inverted and gated via N-6A to N-8D. The "1" side of FF-2 serves as a strobe for gates N-6B, N-6D, N-7B, N-7D, N-8B, and N-8D, and thus, whether or not these gates are open. FF-2 is in the "1" state only when a singles count is in progress. The outputs of gates N-6B, N-6D, N-7B, and N-7D are OR'ed with the four coincidence lines into the inputs of scalers 1 to 4. The outputs of gates N-8B and N-8D are always the inputs of scalers 5 and 6 respectively.

FF-1, FF-2 and M-1 form the control logic for a singles sweep. These two flip-flops are cleared via the CLEAR 6 line, and when in this state FF-2 holds the singles gates shut. At the end of a cycle a coincidence readout is performed, and the RETURN pulse then generated appears at the clock input of FF-1. This flip-flop toggles into the "1" state, opening the gates on FF-2. The first SINGLES SWEEP pulse to appear at the clock input toggles the flip-

flop back into the "0" state, closing the singles gates. As the "1" side of FF-2 falls to gnd., M-1 is triggered and a READ command is generated. At the end of this read-out, a second RETURN pulse is generated, and toggles FF-1 into the "0" state. This disables the gates on FF-2 and completes the singles sweep. If the SINGLES switch is in the OUT position, the first RETURN pulse never appears at the clock input of FF-1 to initiate a singles sweep. Gate N-9B ensures that the coincidence gates can never be open when the singles gates are.

FF-3, FF-4, and N-9C make up the logic which controls the coincidence gates on IM and AC cycles. The two flip-flops are cleared by the CLEAR 6 line, and the "1" side of FF-4 holds the coinc. gates closed. With the SCM switch set to the OUT position, and the SINGLES switch to IN, the RETURN pulse generated at the end of a coincidence readout appears at the clock input of FF-3, toggling it into the "1" state. This affects no change in the status of FF-4, and the coincidence gates remain closed. After the singles readout, a second RETURN pulse appears at the clock input of FF-3 returning it to the "0" state. As it does so, FF-4 toggles into the "1" state, opening the coincidence gates. At the end of the cycle, an E of C pulse appears at the input of N-9C which inverts it and applies it to the clear line of

FF-3 and FF-4. This closes the coincidence gates. During and IM cycle these gates are constantly being shut and reopened by FF-1 on Card 2. The two diodes (1N34) allow either that flip-flop or FF-4 on this card to close the coincidence gates.

With both the SCM and SINGLES switches set to the OUT position, the RETURN pulse generated after a coincidence readout is directed to the set terminal of FF-4, immediately reopening the coincidence gates. These gates are closed at the end of a cycle by an E of C pulse.

With the SCM switch set to IN and the GATES switch set to SCM, the coincidence gates are controlled solely by FF-13 on Card 2, in a manner already described.

CARD 4: (see Figure 14)

This card contains the logic which controls a readout. Normally all flip-flops are in the "0" state, except FF-1 and FF-8 which have no clear lines. FF-15 is cleared by the CLEAR 7 line and it holds down the clear terminals of all other flip-flops (except FF-1 and FF-8). A readout is initiated by a positive E of C pulse, or a negative going READ pulse. The former occurs at the end of a cycle, and results in a coincidence readout. The latter occurs after

a singles sweep, and results in a singles readout. Either one of these pulses results in a negative going pulse at the output of N-1D, which appears at the set terminals of FF-1, FF-8 and FF-15. Since the "1" side of FF-15 is now high, gates N-3A and N-2A are open. FF-1 to FF-7 form a seven bit ring counter, which has as its input CYCLE pulses from gate N-3A. The first CYCLE pulse transfers the "1" from FF-1 to FF-2, and triggers M-1. Strobe lines S7 and S1 are now high. When S1 is high the contents of scaler 1 are presented to the digiplexer (Card 6) and S7 being high results in the first digit of those contents being presented to the BCD to decimal decoder. The CYCLE pulse is delayed 10μs by M-1 and M-2 and then appears at the inputs of gates N-2C and N-2D. These two gates are controlled by FF-14, which is now in the "0" state. Thus the CYCLE pulse appears at terminal "B". The next CYCLE pulse shifts the "1" state from FF-2 to FF-3, and strobe lines S1 and S8 are high. This presents the second digit of scaler 1 to the decoder. Each of the first six CYCLE pulses advances the ring counter one bit to the right, and then appears 10μs later at the terminal labelled "B". In this manner each of the six digits of sealer 1 are presented to the decoder.

The seventh CYCLE pulse to pass through gate N-3A

returns the "1" state from FF-7 back to FF-1. FF-8 to FF-13 make up a six bit right shift register, with the "1" side of FF-7 as its input. As the "1" side of this flip-flop falls to gnd., the "1" state is advanced from FF-8 to FF-9. This brings S2 up, and presents the contents of scaler 2 to the digiplexer. FF-14 toggles into the "1" state as the shift register is advanced, and opens gate N-2C. So, the seventh CYCLE pulse, which has been held up by M-1 and M-2 as the shift register advanced, goes through N-2C and appears at terminal "A". This same pulse is returned via M-3 and M-4 to the clear line of FF-14. The cycle carries on in this manner until the ring counter overflows for the sixth time. By this time the contents of all six scalers have been presented to the digiplexer. As the ring counter overflows for the sixth time, the "1" side of FF-13 falls to gnd, and FF-15 toggles into the "0" state. M-5 triggers as the "1" side of FF-15 falls, and a negative going pulse appears at the output labelled RETURN. Gates N-3A and N-2A are now shut and the readout cycle is complete.

CARD 5: (see Figure 15)

This card generates the typewriter commands and contains the logic to suppress leading zeros. Terminal "C" is simply

the "1" side of FF-15 on Card 4. This line is high during a readout and low otherwise; thus FF-1 is cleared after each readout. This flip-flop controls the gates N-2B and N-1C. Its purpose is to remember whether or not a digit other than zero, in a given six digit number, has been printed. Every seventh CYCLE pulse during a readout appears at terminal "A", passes through two sets of isolation invertors (I-1C, I-1D and I-1E, I-1F) to the clear terminal of FF-1 and to the input of M-3. Thus at the end of each six digit number FF-1 is cleared and a 30ms pulse is directed to the space solenoid driver. All other CYCLE pulses form Card 4 appear at terminal "B", are inverted by N-1A, and directed to the inputs of N-1B, N-1C and N-2B. If the "O" line from the decoder is high, gate N-2D is open and N-1B is shut. If a digit other than "O" has not yet been printed, FF-1 will be in the "O" state, and gate N-2B will be open while N-1C is closed. Thus the CYCLE pulses at terminal "B" are directed to the input of M-3, and a 30ms pulse is applied to the space solenoid driver. As long as the "O" line is high the typewriter will continue to space. If one of the scalers contains a digit other than zero, gate N-2D will shut and N-1B will open. The CYCLE pulse corresponding to that digit will pass through N-1B and trigger M-4. The 30 ms pulse from M-4 is inverted and used as a strobe for gates N-3A to N-5B. The output of one of these gates

(corresponding to the digit other than zero to be printed) will fall to gnd. for the duration of this strobe pulse, while all other outputs will remain high. This fall to gnd. is inverted, and applied to the corresponding typewriter solenoid driver via an emitter follower. At the same time M-1 is triggered, and 10μs later a negative going pulse is applied to the set terminal of FF-1. This opens gate N-1C and closes N-2B. Now all CYCLE pulses appearing at terminal "B" pass through N-1C to the print monostable M-4, regardless of whether or not the digit to be printed is a zero. This procedure continues until the last digit of a scaler is printed, at which time a CYCLE pulse appears at terminal "B", clearing FF-1 and triggering the space monostable M-3. Now that FF-1 is in the "0" state, all zeros will be suppressed until a digit other than zero is encountered. At the end of each readout a RETURN pulse appears at the input of M-5, and a 30ms pulse is directed to the carriage return solenoid driver via B-1B and an emitter follower.

CARD 6: (see Figure 16)

This card contains the logic associated with the multiple input BCD to decimal decoder. The contents of each 24 bit BCD scalers are presented to this card, one at a time,

at a rate determined by the readout control card (Card 4). Of these 24 bits only four are presented to the decoder at any one time. This is accomplished by gates N-1A to N-6D, and strobe lines S7 to S12. These strobe lines are controlled by the ring counter on Card 4. The outputs of these gates are OR'ed into power gates B-1A to B-2B, and then presented to the decoder. Gates N-7A to N-11B and invertors I-1A to I-1D make up the decoder.

As an example, suppose the last digit in scaler 1 is a three. When the contents of this scaler are presented to the digiplexer, the four leftmost inputs will be low, low, high and high respectively. All other inputs will be high. The outputs of gates N-1A to N-6D are normally high, because all strobe lines are normally at gnd. When the contents of scaler 1 are being printed out, S12 will rise to +5 volts briefly (typically 0.2 seconds). During this time, the outputs of N-1A to N-1D will be high, high, low and low respectively, while those of all other gates remain high. The outputs of B-1A to B-2B will be low, low, high and high respectively. The outputs of B-2A and B-2B go directly to two of the inputs of N-8B (the three gate). The outputs of B-1A and B-1B are first inverted by I-1A and I-1B, and then directed to the other two inputs of gate N-8B. Thus all four inputs of N-8B are high for the duration of S12.

An inspection of the schematic shows that no other of the four input gates has all its inputs high at this time. Thus, the only one of these gates to have a low level at its output is N-8B, and this level is inverted by N-12D. So, for the duration of S12, the three line output is high, while all the other outputs are low. As soon as S12 drops to gnd. the three line does so as well.

CARDS 7-11: (see Figure 17)

These five cards are identical (except for clear mechansims) 24 bit, 40Mc BCD scalers. The input is a Schmidt trigger (N-1A to N-1C) which generates pulses of fast fall times (typically 4 volts in 30ns). These pulses are directed to the input of the first decade counter D-1. The six decade counters are arranged to form a simple six digit scaler. All 24 outputs are gated by N-3A to N-8D. These outputs remain high as long as the strobe line is low. When the contents of a scaler are to be printed out, the strobe line of that scaler is raised to +5 volts, and the outputs of D-1 to D-6 are inverted and appear on the 24 output lines. All six scaler are OR'ed in this manner to the 24 inputs of the digiplexer (Card 6). Scalers 1 to 4 have gates N-2A and N-2B on their clear lines, while scaler 5 has only N-2A. Each of these five scalers is

cleared when the previous one is read out. B-1A is necessary because of the high fan-out (24 units), and B-1B is used only because MC832P contains two-power gates. Note that there is no mechanism for clearing the scalers manually, and so the first readout after turn-on should be ignored.

CARD 12: (see Figure 18)

This card contains the sixth scaler and the logic which controls the angular correlation (AC) table. The six digit scaler is identical to those already described (Cards 7-11) except for clear mechanism. This scaler is cleared at the end of a readout by the RETURN pulse via B-1B.

FF-1 and FF-2 form a simple two bit scaler the purpose of which is to initiate an angle change at the completion of every second readout. This scaler is cleared initially by the user at the end of a coincidence readout with the table in the 90° position, by depressing the AC RESET pushbutton on the rear panel. This also clears FF-3 to FF-6. The first three of these flip-flops form a modulo five counter, and the last flip-flop controls the motor direction. At the end of the first coincidence readout M-1 is triggered by FF-2. This monostable generates

an 800ms pulse which is directed to the pin solenoid via an emitter follower. As the pin is raised the motor starts and the angle change begins. When the pin drops M-2 is triggered and generates a 75ms pulse. This pulse toggles FF-3 and is directed to the carriage return solenoid driver via N-3C, N-4C and an emitter follower. During the fifth such angle change, the output of gate N-3D drops, toggling FF-6 and triggering M-4. As FF-6 changes state, the motor direction is reversed and the moveable arm returns to the 180° position. M-4 triggers M-3 45μs later, and this resets the three flip-flops FF-3 to FF-5. Angle changes continue to be performed every other readout, until the 90° position is reached. The next angle change results in another motor direction reversal and the counters are returned to the 90° position.

The second input of M-1 labelled RESTART AC is used as an alternate means of initiating an angle change. This additional angle change is inserted when a position is to be omitted (as is the case when a three angle angular correlation is being performed.) The logic which controls these extra angle changes is described in a later section (see Cards 13 and 14)

IM SWITCH CONTROL: (see Figure 19)

The number of IM switches performed each cycle is

controlled by these two cards (mounted on the bottom of the box, to the left of Card 1). The nuber of switches desired each cycle, is selected via a terminal board on the rear panel.

FF-2 to FF-12 make up a simple 11 bit scaler, which has as its input IM SWEEP pulses. When a predetermined number of switches has occured, all eight inputs of N-2 will be high. The output of this gate then falls to gnd., setting FF-1 to the "1" state and closing gate B-2A. As the "1" side of FF-1 rises the coincidence gates and N-1B are closed. Note that the IM SWEEP pulse which generated this change of state in FF-1, is held up in M-1 and M-2 and then blocked at gate N-1B.

IM switches are inhibited and the coincidence gates remain shut as long as FF-1 is in the "1" state. At the end of either a coincidence or singles readout (depending upon whether or not the SINGLES switch is in the OUT or IN position) the input of M-3 falls to gnd. This E of R signal comes from the "O" side of FF-4 on Card 3. M-3 triggers and a negative going pulse is applied to the clear line of the sealer by B-1B. Thus the output of N-2 rises and gate B-2A opens. The first IM SWEEP pulse to pass through this gate clears FF-1, appears at the input of the scaler, and passes through M-1, M-2, N-1B and N-1C to the IM control logic on Card 2.

The fact that the "1" side of FF-2 is always one of the eight inputs of N-2, combined with the blocking action of M-1, M-2 and N-1B, ensures that an even number of switches and counting periods will take place each cycle.

At start-up, the scaler is set via N-1A and B-2B. This ensures that the output of gate N-2 will be low, and hence that the coincidence gates are closed and the IM switches inhibited during the first "half cycle".

CARDS 13 and 14: (see Figure 20)

Card 13 generates a square wave which is the input to the main clock (Card 1). This square wave is derived either from an external oscillator or a 100cps crystal controlled oscillator. Each of these lines contain a Schmidt trigger, N-5A, N-5B, and N-5C in one case and N-6A, N-6B and N-6C in the other. When FF-2 is in the "1" state, as is usually the case, N-7A is closed and N-7C open. This routes the 100cps signal from the crystal controlled oscillator through N-7B to the output of this card. When the user depresses the AUTO START pushbutton on the rear panel FF-2 is cleared, and N-7C closes and N-7A opens. This routes the external oscillator signal through N-7B to the output of this card. At the end of a cycle, FF-2 is set by an E of C pulse and the crystal controlled oscillator becomes the main clock.

Card 14 contains the logic which, during an angular correlation run, decides which table positions are to be used. Mounted on the rear panel are five toggle switches, one for each angel. A switch in the down position will result in that particular position being omitted. At the beginning of an angle change, a PIN LIFT pulse appears at the input of N-1C. This is inverted and directed to the clear line of the four digit BCD counter (D-1 to D-4) and the reset terminal of FF-1. As FF-1 is cleared N-1A closes and the clock pulses to the main clock (Card 1) are blocked. N-1B opens and clock pulses are directed to the input of the four digit counter. Approximately five seconds after a pin lift the STROBE pulse is generated, and appears at one of the inputs of gates N-2A, N-2B, N-3A, N-3B and N-4A. If any one of these gates is open at this time (this indicates that a desired counter position has been reached) the STROBE pulse will be inverted and appear at the set terminal of FF-1. This closes N-1B, stopping the four digit counter, and opens N-1A, which starts the main clock (Card 1). If none of these gates are open (which means that this counter position is to be omitted) the STROBE pulse does not set FF-1 and the four digit scaler continues to count until all the inputs of N-4B are high. With the jumpers as shown in the schematic this condition will be achieved approximately 30 seconds after

the pin lift which initiated the angle change. At this time a negative going level change appears at the output labelled RESTART AC. This appears at the input of M-1 on Card 12 and results in another angle change being performed. The resulting PIN LIFT pulse clears the four digit scaler. If after 30 seconds a desired position has not been reached, another angle change will occur. This procedure will continue until a desired position is reached and FF-1 is set by the STROBE pulse.

CARDS 15 and 16: (see Figure 21)

These two cards contain the logic which outputs the detector position on the typewriter during an angular correlation run. All carriage return signals generated by readout control (Card 4) and AC control (Card 12) appear at the input labelled RETURN. These are directed to the carriage return solenoid driver via N-2A, N-2D, and an emitter follower. As an angle change is initiated a positive pulse appears at the input labelled PIN LIFT. The trailing edge of this signal is sharpened up by the Schmidt trigger (N-1A, N-1B and N-1C) and used to trigger M-1. Approximately five seconds later M-2 and M-4 are triggered. The output of M-4 is used as a strobe for gates N-3B, N-4B,

N-5B, N-6B and N-7B. One of these gates (corresponding to the current table position) will be open, and this strobe pulse will be directed to the appropriate typewriter key driver. Approximately 250ms after this key is struck, M-3 will fire and this pulse is directed to the carriage return solenoid driver via N-2B, N-2D and an emitter follower

Figure 11: Schematic for Card 1; the main clock.

Front Connector		Rear Connector	
1-	Cycle	1-	+5 volts
2-	E. of C. from	2-	Gnd
3-	IM tap	3-	Clock Enable
4-	Singles switches	4-	Cycle
5-	Motor	5-	E. of C.
6-	Input	6-	Im Sweep
7-	Clear 1	7-	Singles Sweep
8-	T4	8-	Motor-on Time
9-	T5	9-	
10-	T6	10-	
11-	T9	11-	
12-	T10	12-	
13-	T11	13-	
14-	T12	14-	
15-	T13	15-	
16-	T14	16-	
17-	T15	17-	
18-	T16	18-	
19-	T17	19-	
20-	T18	20-	
21-	T19	21-	
22-	T20	22-	

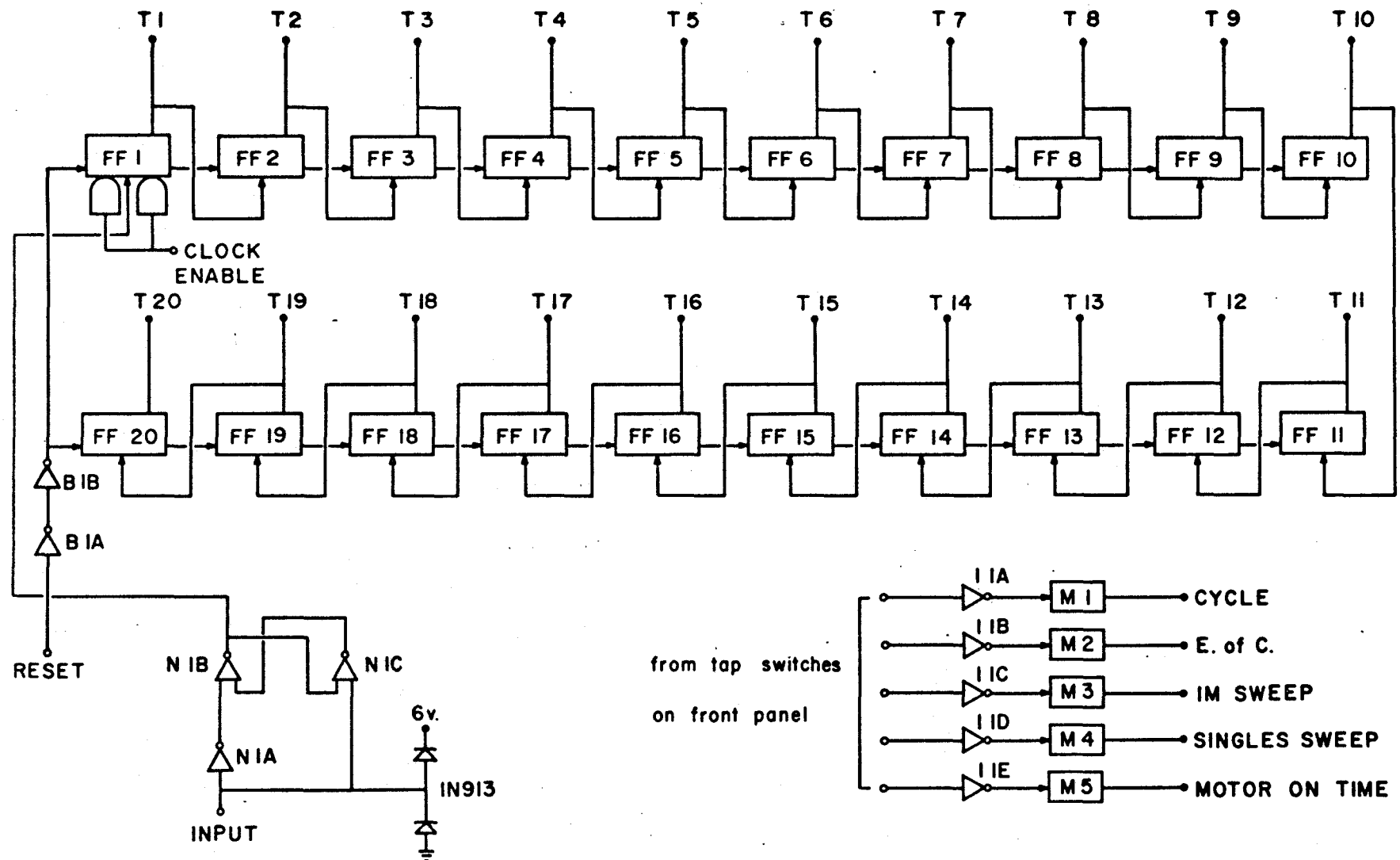
T1
T2
T3
T4
T5
T6
T7
T8
T9
T10
FF 1
FF 2
FF 3
FF 4
FF 5
FF 6
FF 7
FF 8
FF 9
FF 10
CLOCK ENABLE
T20
T19
T18
T17
T16
T15
T14
T13
T12
T11
FF 20
FF 19
FF 18
FF 17
FF 16
FF 15
FF 14
FF 13
FF 12
FF 11
B 1B
B 1A
RESET
N 1B
N 1C
N 1A
6v.
IN913
INPUT
from tap switches on front panel
1 1A
1 1B
1 1C
1 1D
1 1E
M 1
M 2
M 3
M 4
M 5
CYCLE
E. of C.
IM SWEEP
SINGLES SWEEP
MOTOR ON TIME

Figure 12: Schematic for Card 2; AC, IM and SCM control.

FRONT CONNECTOR

1- Chance 1:1
2- Chance 1:3
3- Chance 1:7
4- Chance 1:15
5- Im Cycle In-Out
6- Chance In
7-
8- Clear 2
9- Clear 3
10- Clear 4
11- Clear 5
12-
13- SCM MD
14-
15-
16- Pause
17- Start
18- Im. FD.
19- SCM FD
20- FD (in)
21- To SCM In-Out
22- From SCM In-Out

REAR CONNECTOR

1- +5 volts
2- Gnd
3- Clock Enable
4- Cycle
5- E. of C.
6- IM Sweep
7-
8- Motor-on Time
9- Chance (to SCA's)
10- Coinc. Gates IM
11- To MD. Relay
12- To M. Relay
13- To FD. Relay
14- S. Up
15- Coinc Gates SCM
16-
17-
18-
19-
20-
21-
22-

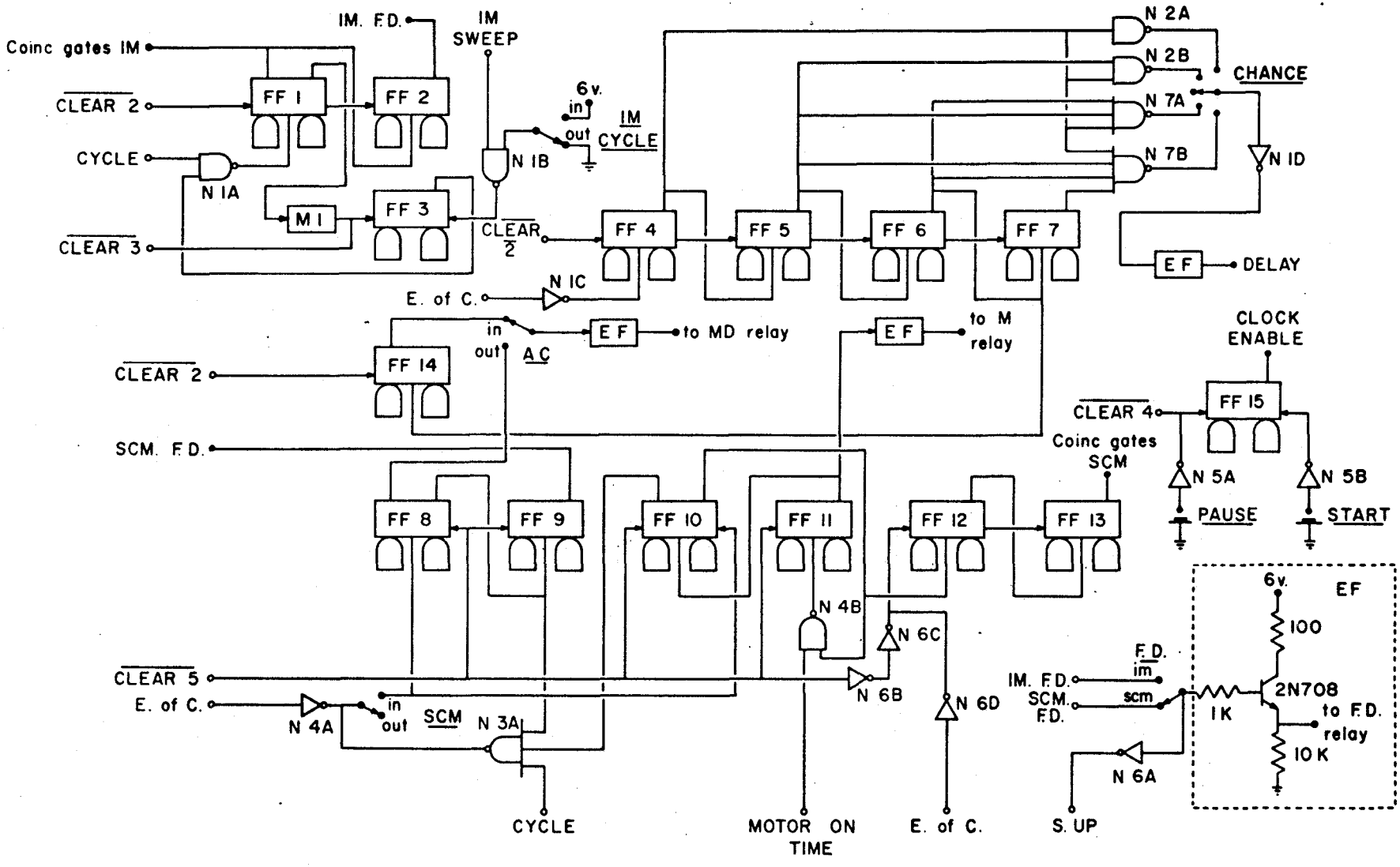
Coinc gates IM
CLEAR 2
CYCLE
N 1A
CLEAR 3
FF 1
FF 2
M 1
FF 3
IM. F.D.
IM SWEEP
N 1B
6v.
in
out
IM CYCLE
CLEAR 2
FF 4
FF 5
FF 6
FF 7
N 2A
N 2B
N 7A
N 7B
CHANCE
N 1D
E F
DELAY
E. of C.
N 1C
in
out
A C
E F
to MD relay
E F
to M relay
CLEAR 2
FF 14
SCM. F.D.
CLOCK ENABLE
CLEAR 4
FF 15
Coinc gates SCM
N 5A
N 5B
PAUSE
START
FF 8
FF 9
FF 10
FF 11
FF 12
FF 13
N 4B
N 6C
N 6B
N 6D
CLEAR 5
E. of C.
N 4A
in
out
SCM
N 3A
CYCLE
MOTOR ON TIME
E. of C.
S. UP
F.D. im
IM. F.D.
SCM. F.D.
scm
N 6A
6v.
EF
100
2N708
1K
to F.D. relay
10 K

Figure 13: Schematic for Card 3; input amplifiers and gates.

FRONT CONNECTOR	REAR CONNECTOR
1- Coinc 1	1- +5 Volts
2- Coinc 2	2- Gnd
3- Coinc 3	3- Read
4- Coinc 4	4-
5- Singles 1	5- E. of C.
6- Singles 2	6-
7- Singles 3	7- Singles Sweep
8- Singles 4	8- Return
9- Singles 5	9-
10- Singles 6	10- Coinc Gates IM
11-	11-
12- Clear 6	12-
13- -7 volts	13-
14-	14- S. Up
15- To Singles In-Out	15- Coinc Gates SCM
16- From Singles In	16-
17- From Singles Out-In	17- To Scaler 1
18-	18- To Scaler 2
19- From Singles Out	19- To Scaler 3
20- Coinc. Gates Normal	20- To Scaler 4
21- Coinc. Gates SCM	21- To Scaler 5
22- Coinc. Gates (in)	22- To Scaler 6

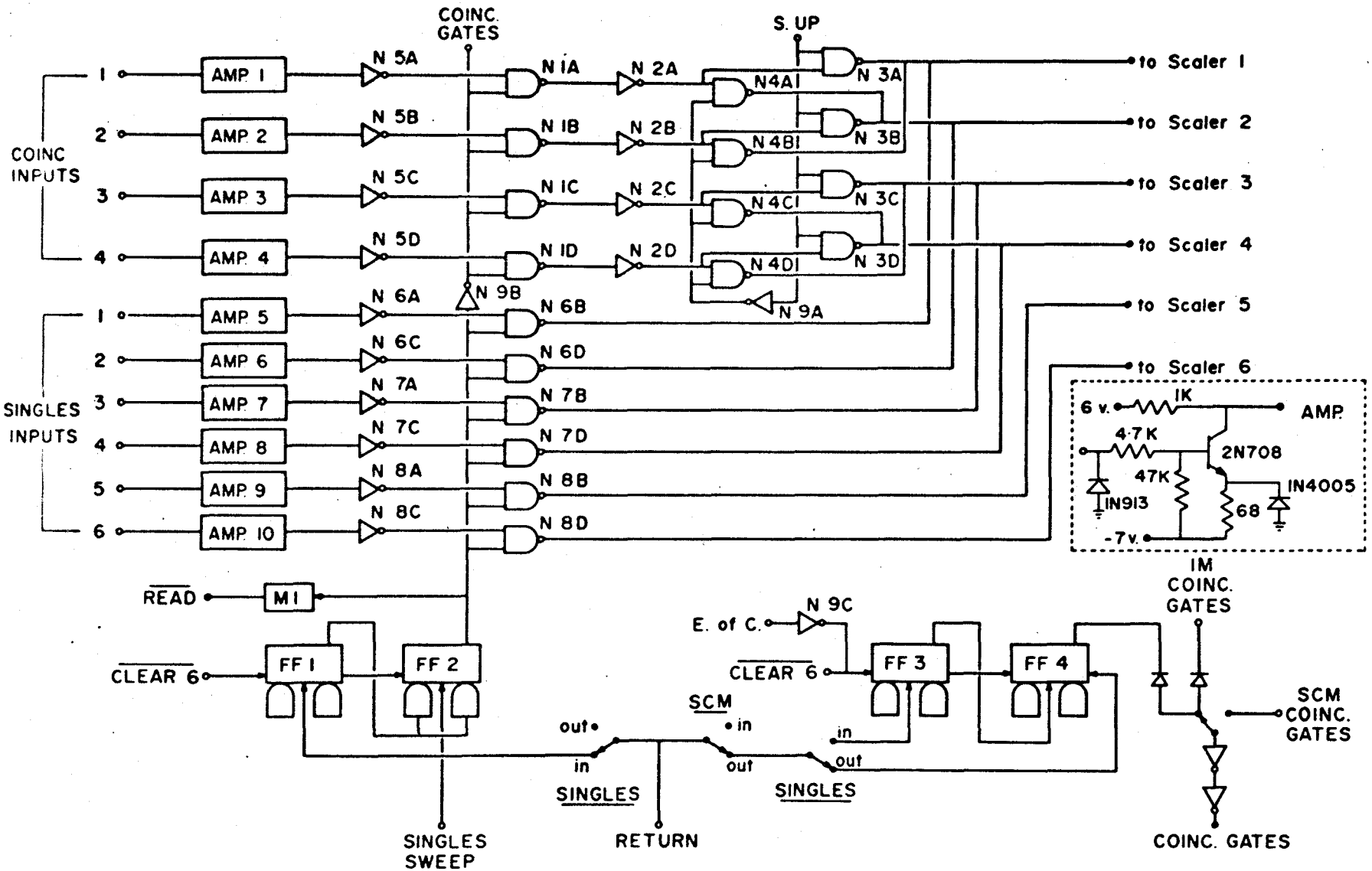
COINC. GATES
S. UP
COINC INPUTS
SINGLES INPUTS
AMP 1
AMP 2
AMP 3
AMP 4
AMP 5
AMP 6
AMP 7
AMP 8
AMP 9
AMP 10
N 5A
N 5B
N 5C
N 5D
N 6A
N 6C
N 7A
N 7C
N 8A
N 8C
N 9B
N 1A
N 1B
N 1C
N 1D
N 2A
N 2B
N 2C
N 2D
N4A
N4B
N4C
N4D
N 3A
N 3B
N 3C
N 3D
N 9A
N 6B
N 6D
N 7B
N 7D
N 8B
N 8D
to Scaler 1
to Scaler 2
to Scaler 3
to Scaler 4
to Scaler 5
to Scaler 6
6 v.
1K
AMP.
4·7K
2N708
47K
IN913
IN4005
68
-7v.
READ
M1
CLEAR 6
FF 1
FF 2
E. of C.
N 9C
FF 3
FF 4
IM COINC. GATES
SCM COINC. GATES
SCM
out
in
SINGLES
RETURN
SINGLES SWEEP
COINC. GATES

Figure 14: Schematic for Card 4; readout control.

FRONT CONNECTOR	REAR CONNECTOR
1-	1- +5 volts
2-	2- Gnd.
3-	3- Read
4-	4- Cycle
5-	5- E. of C.
6-	6- "B"
7-	7- "A"
8-	8- Return
9-	9- "C"
10-	10-
11-	11-
12-	12-
13- Clear 7	13-
14- S1	14-
15- S2	15-
16- S3	16-
17- S4	17-
18- S5	18-
19- S6	19- S7
20- S11	20- S8
21- S12	21- S9
22-	22- S10

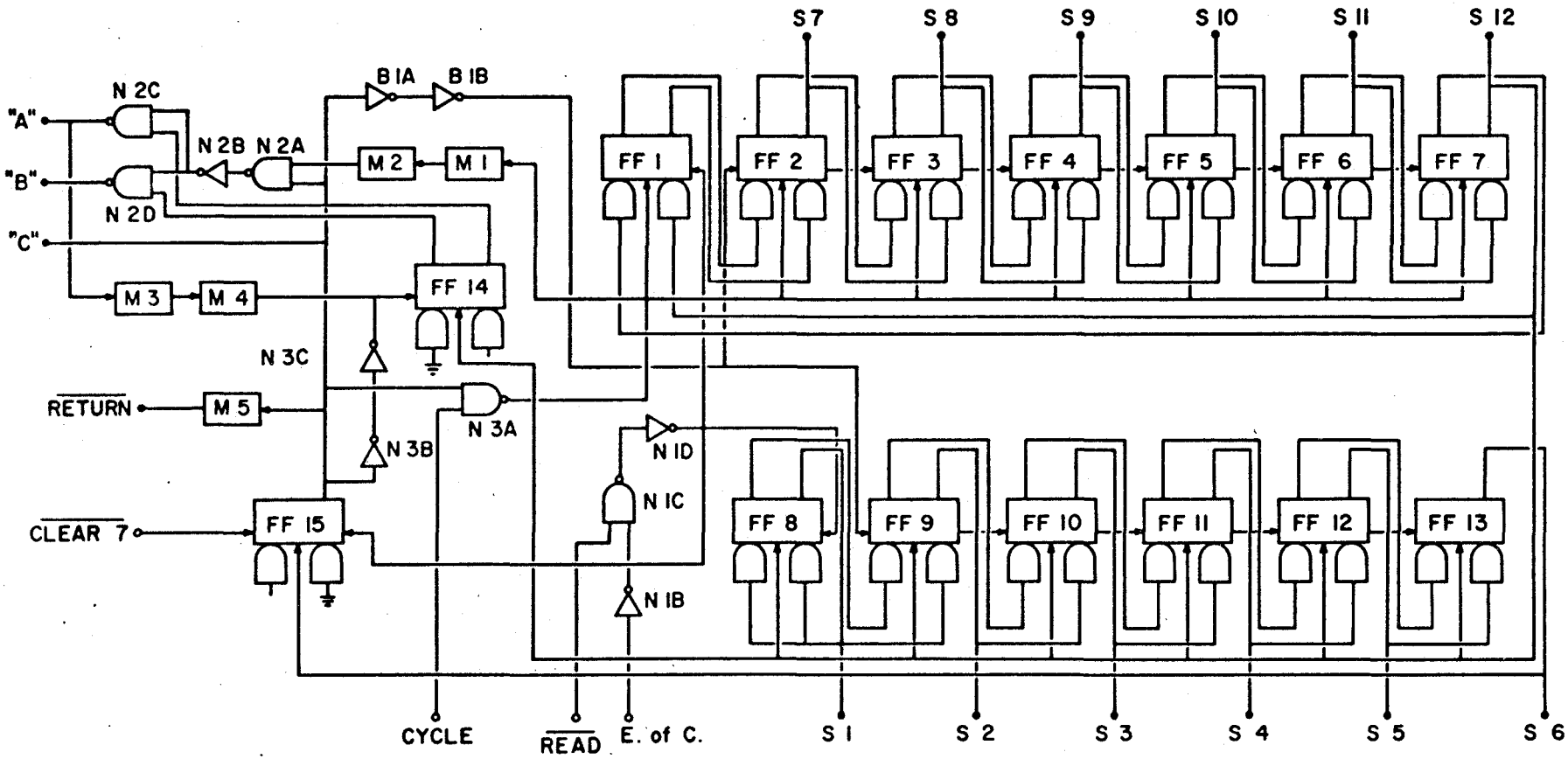
S7
S8
S9
S10
S11
S12
N 2C
"A"
"B"
"C"
N 2B
N 2A
N 2D
B IA
B IB
M 2
M 1
FF 1
FF 2
FF 3
FF 4
FF 5
FF 6
FF 7
M 3
M 4
FF 14
N 3C
RETURN
M 5
N 3A
N 3B
N ID
N IC
N IB
CLEAR 7
FF 15
FF 8
FF 9
FF 10
FF 11
FF 12
FF 13
CYCLE
READ
E. of C.
S 1
S 2
S 3
S 4
S 5
S 6

Figure 15: Schematic for Card 5; zero suppress and solenoid drivers.

FRONT CONNECTOR	REAR CONNECTOR
1- 0 (in)	1- +5 volts
2- 1 (in)	2- Gnd.
3- 2 (in)	3-
4- 3 (in)	4-
5- 4 (in)	5- E. of C.
6- 5 (in)	6- "B"
7- 6 (in)	7- "A"
8- 7 (in)	8- Return
9- 8 (in)	9- "C"
10- 9 (in)	10- To 0 Solenoid Driver
11-	11- To 1 Solenoid Driver
12- To AC Out-In	12- To 2 Solenoid Driver
13- From AC Out-In	13- To 3 Solenoid Driver
14- +5 volts	14- To 4 Solenoid Driver
15- Gnd.	15- To 5 Solenoid Driver
16-	16- To 6 Solenoid Driver
17-	17- To 7 Solenoid Driver
18- Cycle Out-In	18- To 8 Solenoid Driver
19-	19- To 9 Solenoid Driver
20-	20- To Space Solenoid Driver
21-	21- To Carriage Solenoid Driver
22-	22-

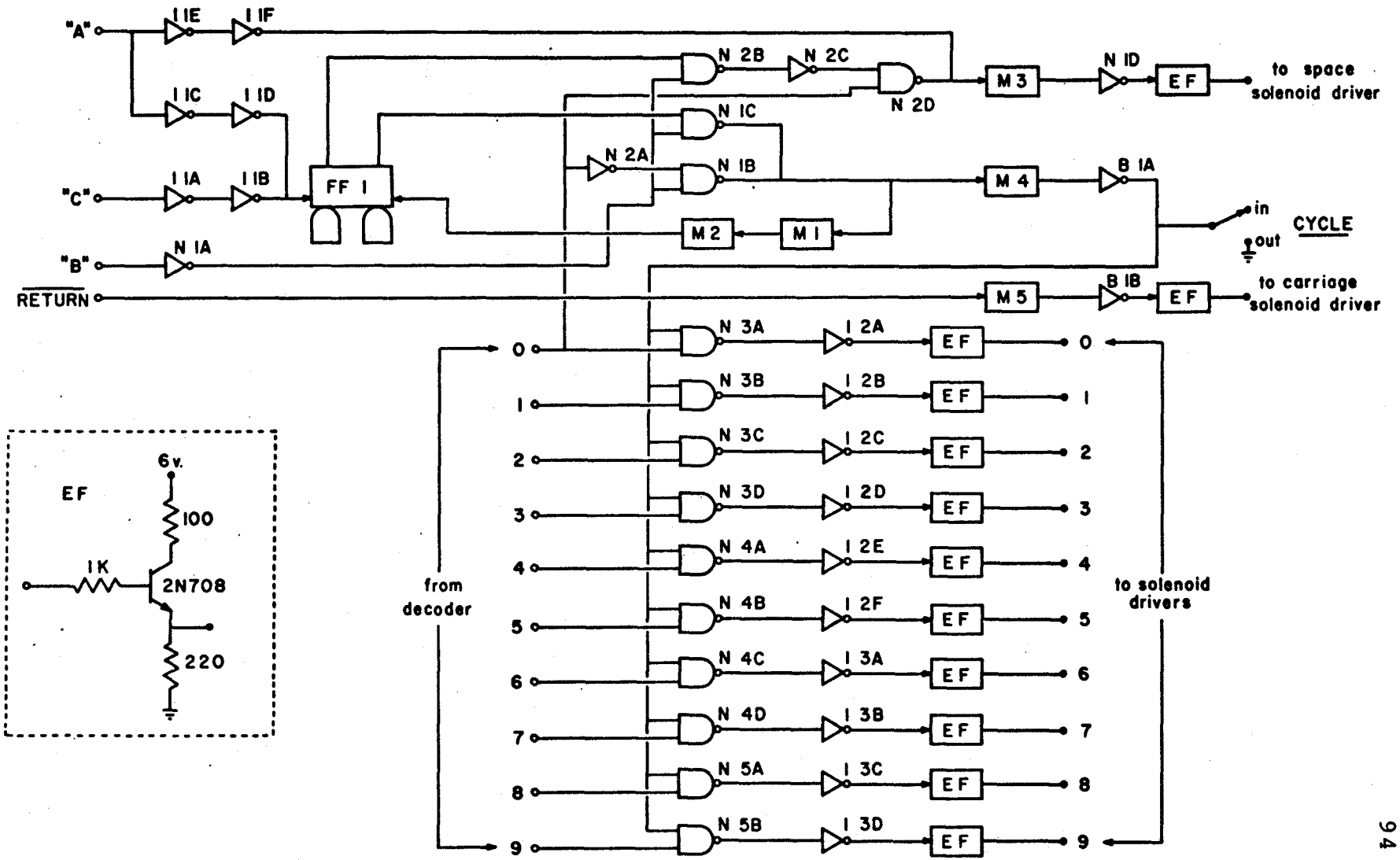
"A"
"C"
"B"
RETURN
I IE
I IF
I IC
I ID
I IA
I IB
N IA
FF I
N 2B
N 2C
N 2D
N IC
N 2A
N IB
M 2
M I
M 3
M 4
M 5
N ID
B IA
B IB
EF
to space solenoid driver
in
out
CYCLE
to carriage solenoid driver
from decoder
to solenoid drivers
N 3A
I 2A
N 3B
I 2B
N 3C
I 2C
N 3D
I 2D
N 4A
I 2E
N 4B
I 2F
N 4C
I 3A
N 4D
I 3B
N 5A
I 3C
N 5B
I 3D
0
1
2
3
4
5
6
7
8
9
6v.
100
1K
2N708
220

Figure 16: Schematic for Card 6; the digiplexer and decoder.

FRONT CONNECTOR	REAR CONNECTOR
1- 0 (out)	1- +5 volts
2- 1 (out)	2- Gnd.
3- 2 (out)	3- Bit 9
4- 3 (out)	4- Bit 10
5- 4 (out)	5- Bit 11
6- 5 (out)	6- Bit 12
7- 6 (out)	7- Bit 13
8- 7 (out)	8- Bit 14
9- 8 (out)	9- Bit 15
10- 9 (out)	10- Bit 16
11-	11- Bit 17
12- Bit 1	12- Bit 18
13- Bit 2	13- Bit 19
14- Bit 3	14- Bit 20
15- Bit 4	15- Bit 21
16- Bit 5	16- Bit 22
17- Bit 6	17- Bit 23
18- Bit 7	18- Bit 24
19- Bit 8	19- S7
20- S11	20- S8
21- S12	21- S9
22-	22- S10

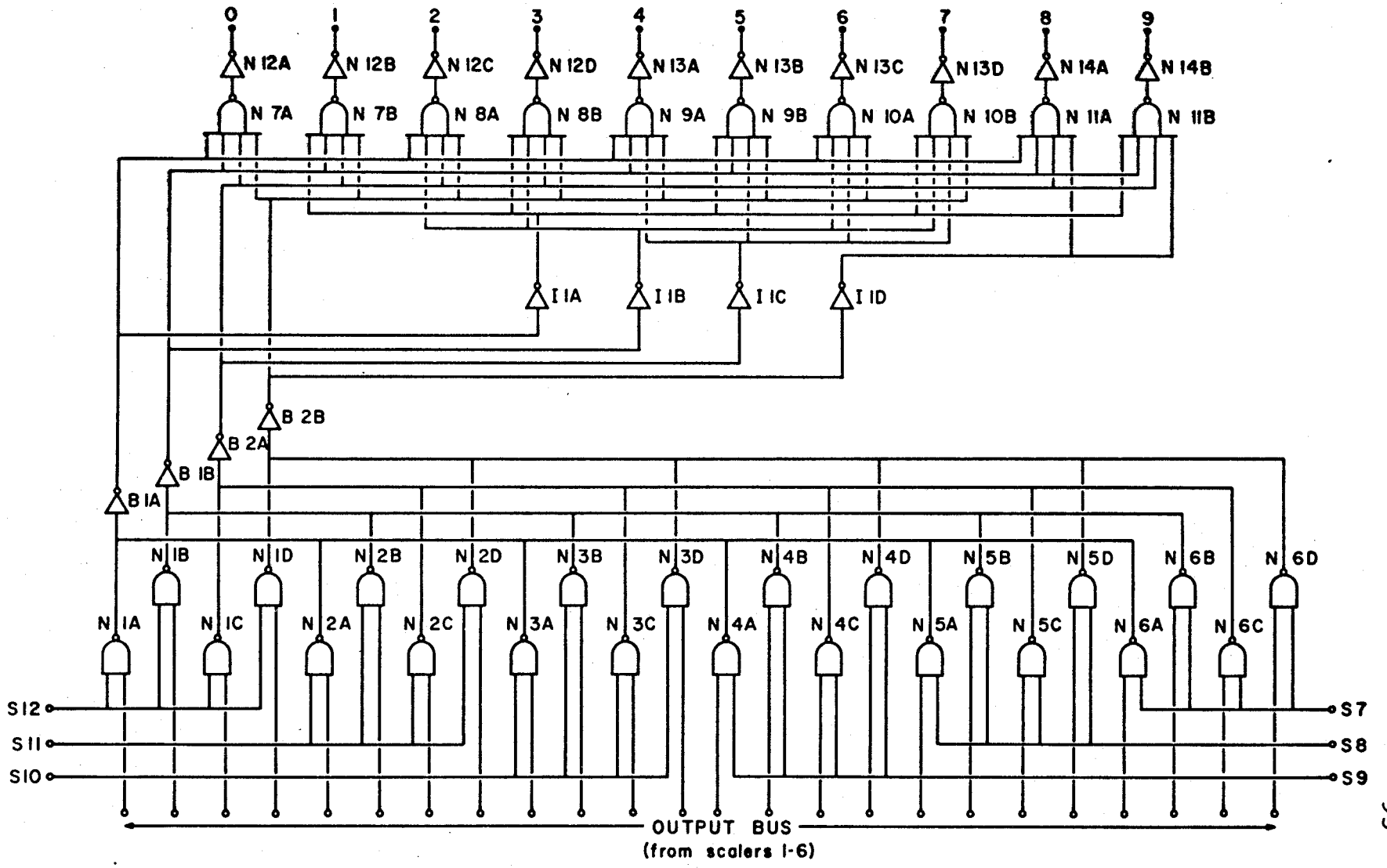
0
1
2
3
4
5
6
7
8
9
N 12A
N 12B
N 12C
N 12D
N 13A
N 13B
N 13C
N 13D
N 14A
N 14B
N 7A
N 7B
N 8A
N 8B
N 9A
N 9B
N 10A
N 10B
N 11A
N 11B
I 1A
I 1B
I 1C
I 1D
B 2B
B 2A
B 1B
B 1A
N 1B
N 1D
N 2B
N 2D
N 3B
N 3D
N 4B
N 4D
N 5B
N 5D
N 6B
N 6D
N 1A
N 1C
N 2A
N 2C
N 3A
N 3C
N 4A
N 4C
N 5A
N 5C
N 6A
N 6C
S12
S11
S10
S7
S8
S9
OUTPUT BUS
(from scalers 1-6)

Figure 17: Schematic for cards 7-11; 24 bit BCD scalers.

FRONT CONNECTOR	REAR CONNECTOR
1-	1- +5 volts
2-	2- Gnd.
3-	3- Bit 9
4-	4- Bit 10
5-	5- Bit 11
6-	6- Bit 12
7-	7- Bit 13
8-	8- Bit 14
9-	9- Bit 15
10-	10- Bit 16
11-	11- Bit 17
12- Bit 1	12- Bit 18
13- Bit 2	13- Bit 19
14- Bit 3	14- Bit 20
15- Bit 4	15- Bit 21
16- Bit 5	16- Bit 22
17- Bit 6	17- Bit 23
18- Bit 7	18- Bit 24
19- Bit 8	19-
20-	20-
21- S2 to S6 (clear)	21-
22- S1 to S5 (strobe)	22- Input

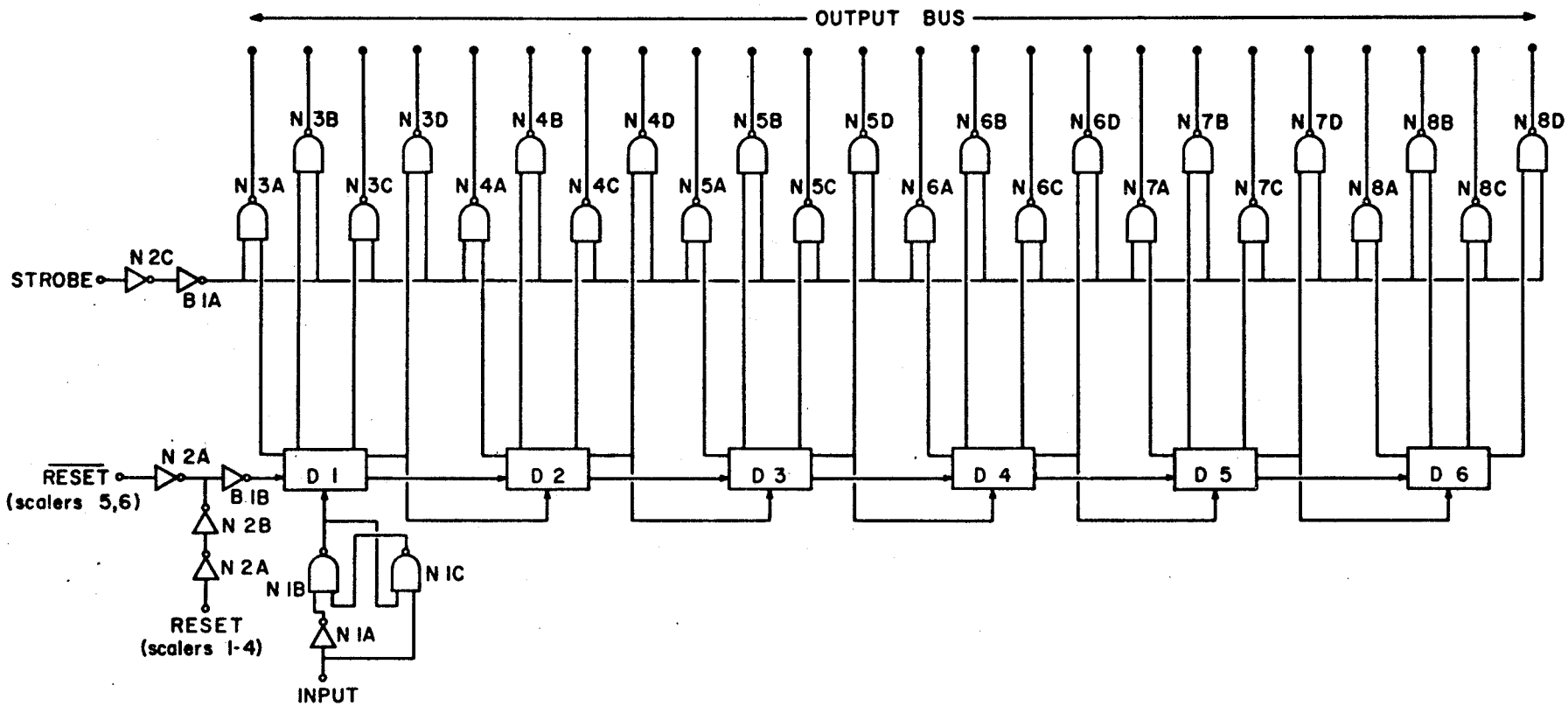
OUTPUT BUS
N 3A
N 3B
N 3C
N 3D
N 4A
N 4B
N 4C
N 4D
N 5A
N 5B
N 5C
N 5D
N 6A
N 6B
N 6C
N 6D
N 7A
N 7B
N 7C
N 7D
N 8A
N 8B
N 8C
N 8D
STROBE
N 2C
B IA
RESET (scalers 5,6)
N 2A
B IB
N 2B
N 2A
RESET (scalers 1-4)
D 1
D 2
D 3
D 4
D 5
D 6
N IB
N IC
N IA
INPUT

Figure 18: Schematic for card 12; one scaler and AC table control.

FRONT CONNECTOR	REAR CONNECTOR	TOP CONNECTOR
1-	1- +5 volts	1- MD
2-	2- Gnd.	2- Return (out)
3-	3- Bit 9	3- Pin Solenoid
4-	4- Bit 10	4-
5-	5- Bit 11	5-
6-	6- Bit 12	6-
7-	7- Bit 13	7-
8-	8- Bit 14	8-
9-	9- Bit 15	9-
10-	10- Bit 16	10-
11-	11- Bit 17	11-
12- Bit 1	12- Bit 18	12-
13- Bit 2	13- Bit 19	13-
14- Bit 3	14- Bit 20	14-
15- Bit 4	15- Bit 21	15-
16- Bit 5	16- Bit 22	16-
17- Bit 6	17- Bit 23	17-
18- Bit 7	18- Bit 24	18-
19- Bit 8	19-	19-
20-	20-	20- AC. Reset
21-	21-	21- AC In-Out
22- S6	22- Input	22- Return (in)

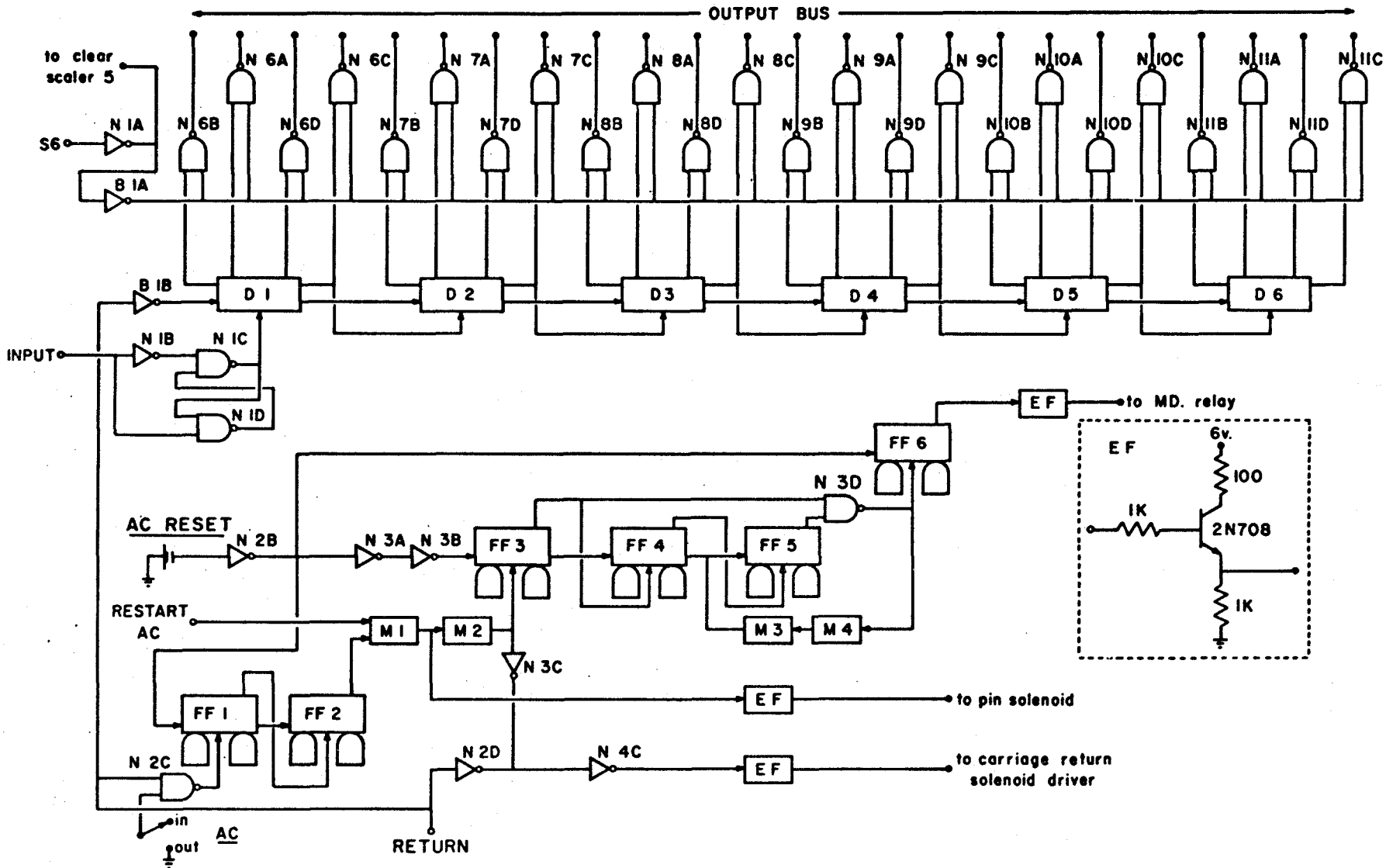
OUTPUT BUS
to clear scaler 5
S6
N 1A
B 1A
N 6B
N 6A
N 6D
N 6C
N 7B
N 7A
N 7D
N 7C
N 8B
N 8A
N 8D
N 8C
N 9B
N 9A
N 9D
N 9C
N 10B
N 10A
N 10D
N 10C
N 11B
N 11A
N 11D
N 11C
B 1B
D 1
D 2
D 3
D 4
D 5
D 6
INPUT
N 1B
N 1C
N 1D
E F
to MD. relay
FF 6
N 3D
AC RESET
N 2B
N 3A
N 3B
FF 3
FF 4
FF 5
RESTART AC
M 1
M 2
M 3
M 4
N 3C
FF 1
FF 2
E F
to pin solenoid
N 2C
N 2D
N 4C
E F
to carriage return solenoid driver
in
out
AC
RETURN
E F
6v.
100
1K
2N708
1K

Figure 19: Schematic for IM switch control.

CONNECTOR ON CARD I	CONNECTOR ON CARD II
1- 7	1- IM Sweep (in)
2- 6	2- Out
3- 5	3- Set
4- Out	4-
5- 4	5- Input
6- 3	6- Clear
7- 2	7-
8- 1	8- Coinc. Gates Normal
9- 1024	9-
10- 512	10-
11- 256	11-
12- 128	12- Clear 8
13- 64	13-
14- 32	14-
15- 16	15- IM Sweep (out)
16- 8	16-
17- 4	17-
18- Set	18-
19- Gnd.	19- Gnd.
20- +5 volts	20- +5 volts
21- Clear	21-
22- Input	22- E. of R.

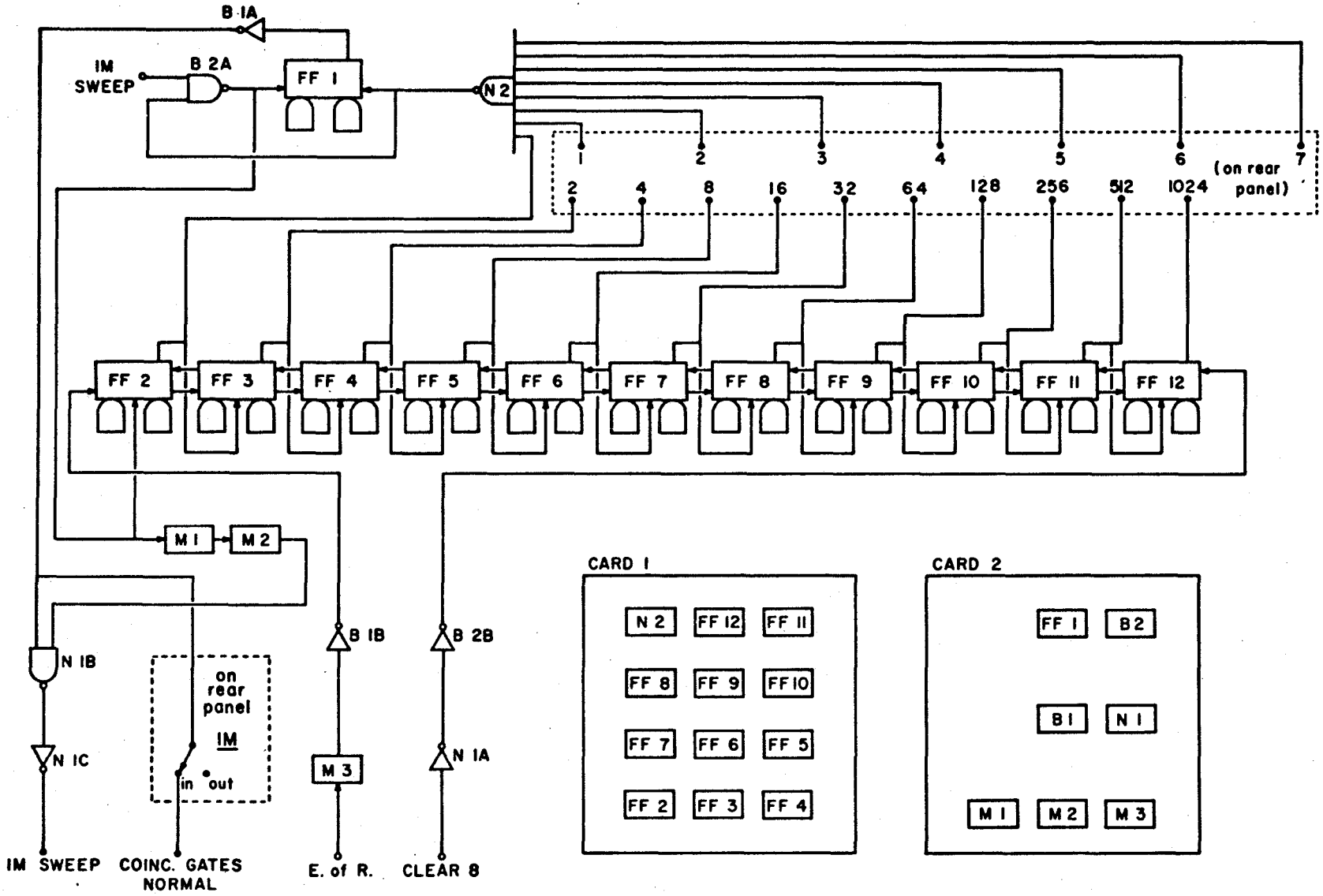
B 1A
IM SWEEP
B 2A
FF 1
N 2
1
2
3
4
5
6
7
(on rear panel)
2
4
8
16
32
64
128
256
512
1024
FF 2
FF 3
FF 4
FF 5
FF 6
FF 7
FF 8
FF 9
FF 10
FF 11
FF 12
M 1
M 2
N 1B
N 1C
on rear panel
IM
in
out
B 1B
B 2B
M 3
N 1A
IM SWEEP
COINC. GATES NORMAL
E. of R.
CLEAR 8
CARD 1
N 2
FF 12
FF 11
FF 8
FF 9
FF 10
FF 7
FF 6
FF 5
FF 2
FF 3
FF 4
CARD 2
FF 1
B 2
B 1
N 1
M 1
M 2
M 3

Figure 20: Schematic for cards 13 and 14; main clock control.

CONNECTOR ON CARD 13	CONNECTOR ON CARD 14
1- Gnd.	1- +5 volts
2- +5 volts	2- Gnd.
3-	3-
4-	4- Restart AC
5-	5- Strobe
6-	6-
7-	7- Clock (in)
8-	8- Pin Lift
9-	9- Reset
10-	10- Clock (out)
11-	11- 90
12-	12- $112\frac{1}{2}$
13-	13- 135
14-	14- $157\frac{1}{2}$
15-	15- 180
16-	16- 1
17-	17- 2
18-	18- 3
19- Ext. Osc.	19- 4
20- Auto Start	20- 5
21- E. of C.	21-
22- Clock (out)	22-

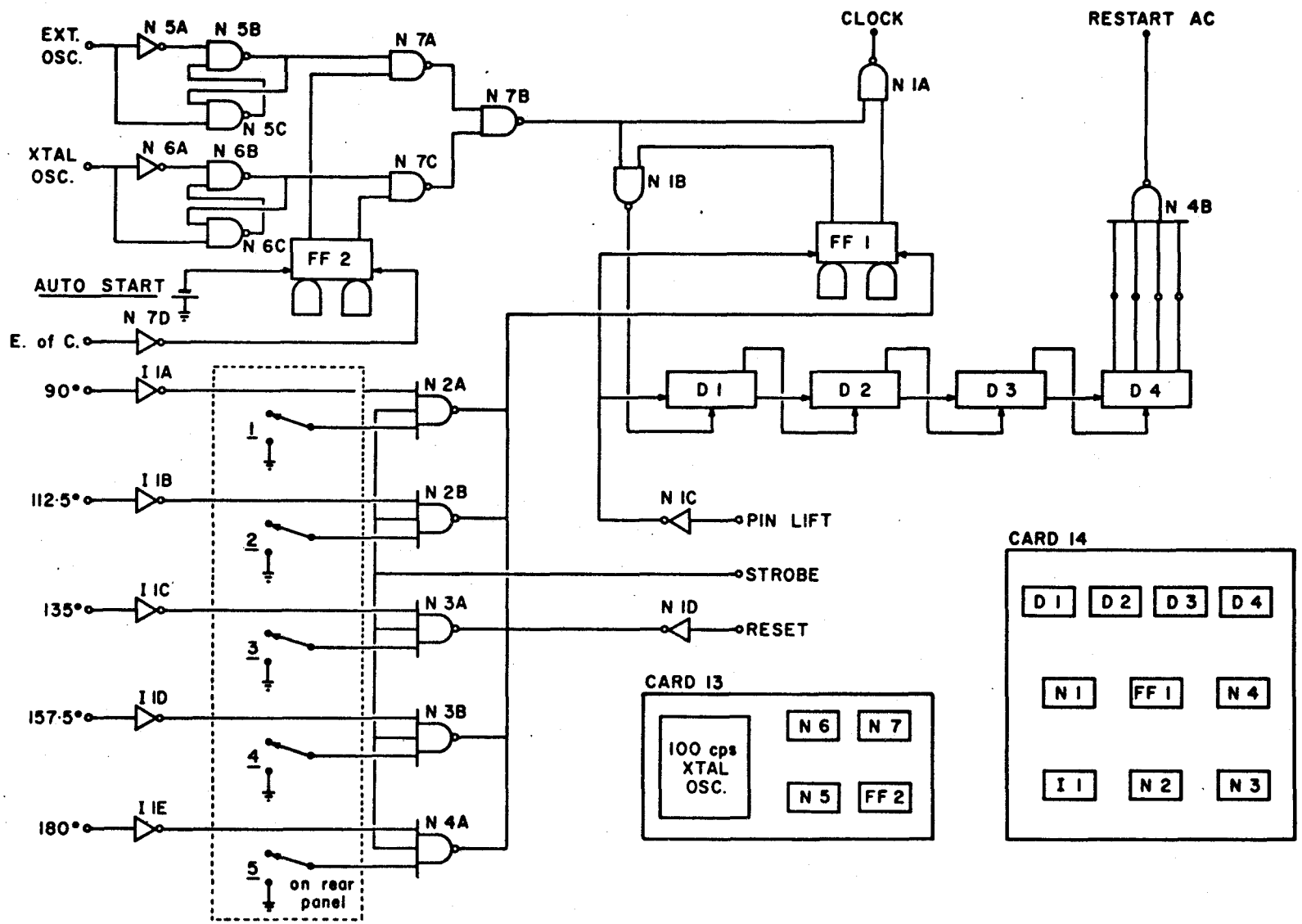
EXT. OSC.
N 5A
N 5B
N 5C
N 7A
N 7B
XTAL OSC.
N 6A
N 6B
N 6C
N 7C
FF 2
AUTO START
N 7D
E. of C.
CLOCK
N 1A
N 1B
FF 1
RESTART AC
N 4B
D 1
D 2
D 3
D 4
I 1A
90°
1
N 2A
I 1B
112·5°
2
N 2B
N 1C
PIN LIFT
STROBE
I 1C
135°
3
N 3A
N 1D
RESET
I 1D
157·5°
4
N 3B
I 1E
180°
5
on rear panel
N 4A
CARD 13
100 cps XTAL OSC.
N 6
N 7
N 5
FF 2
CARD 14
D 1
D 2
D 3
D 4
N 1
FF 1
N 4
I 1
N 2
N 3

Figure 21: Schematic for cards 15 and 16; angle indicator print control.

CONNECTOR ON CARD 15	CONNECTOR ON CARD 16
1- +5 volts	1- 90°
2-	2- +5 volts
3-	3- Gnd.
4-	4- 1 Line
5-	5- To 1 Key Driver
6-	6- $112\frac{1}{2}°$
7-	7- 2 Line
8- Gnd.	8- To 2 Key Driver
9-	9- 135°
10-	10- 3 Line
11- Return (in)	11- To 3 Key Driver
12- Pin Lift	12-
13- Return (out)	13- $157\frac{1}{2}°$
14-	14- 4 Line
15-	15- To 4 Key Driver
16- Strobe	16-
17-	17-
18-	18-
19-	19- Strobe
20-	20- 180°
21-	21- 5 Line
22-	22- To 5 Key Driver

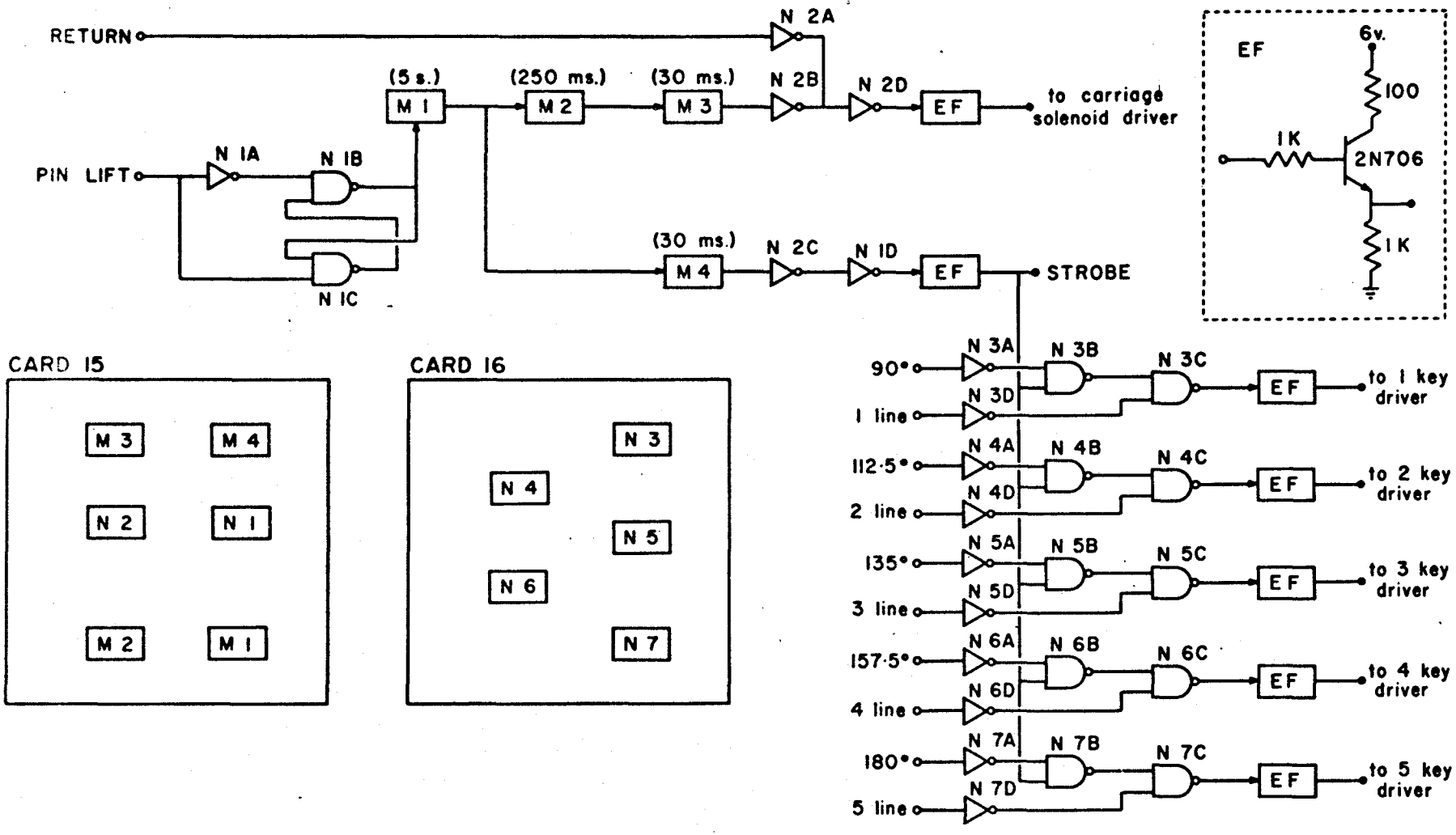
RETURN
N 2A
(5 s.)
M 1
(250 ms.)
M 2
(30 ms.)
M 3
N 2B
N 2D
EF
to carriage solenoid driver
PIN LIFT
N 1A
N 1B
N 1C
(30 ms.)
M 4
N 2C
N 1D
EF
STROBE
EF
6v.
100
1K
2N706
1K
CARD 15
M 3
M 4
N 2
N 1
M 2
M 1
CARD 16
N 3
N 4
N 5
N 6
N 7
90°
1 line
N 3A
N 3B
N 3C
N 3D
EF
to 1 key driver
112·5°
2 line
N 4A
N 4B
N 4C
N 4D
EF
to 2 key driver
135°
3 line
N 5A
N 5B
N 5C
N 5D
EF
to 3 key driver
157·5°
4 line
N 6A
N 6B
N 6C
N 6D
EF
to 4 key driver
180°
5 line
N 7A
N 7B
N 7C
N 7D
EF
to 5 key driver

Figure 22: Integrated circuit layout for cards 1,2,3, and 4.

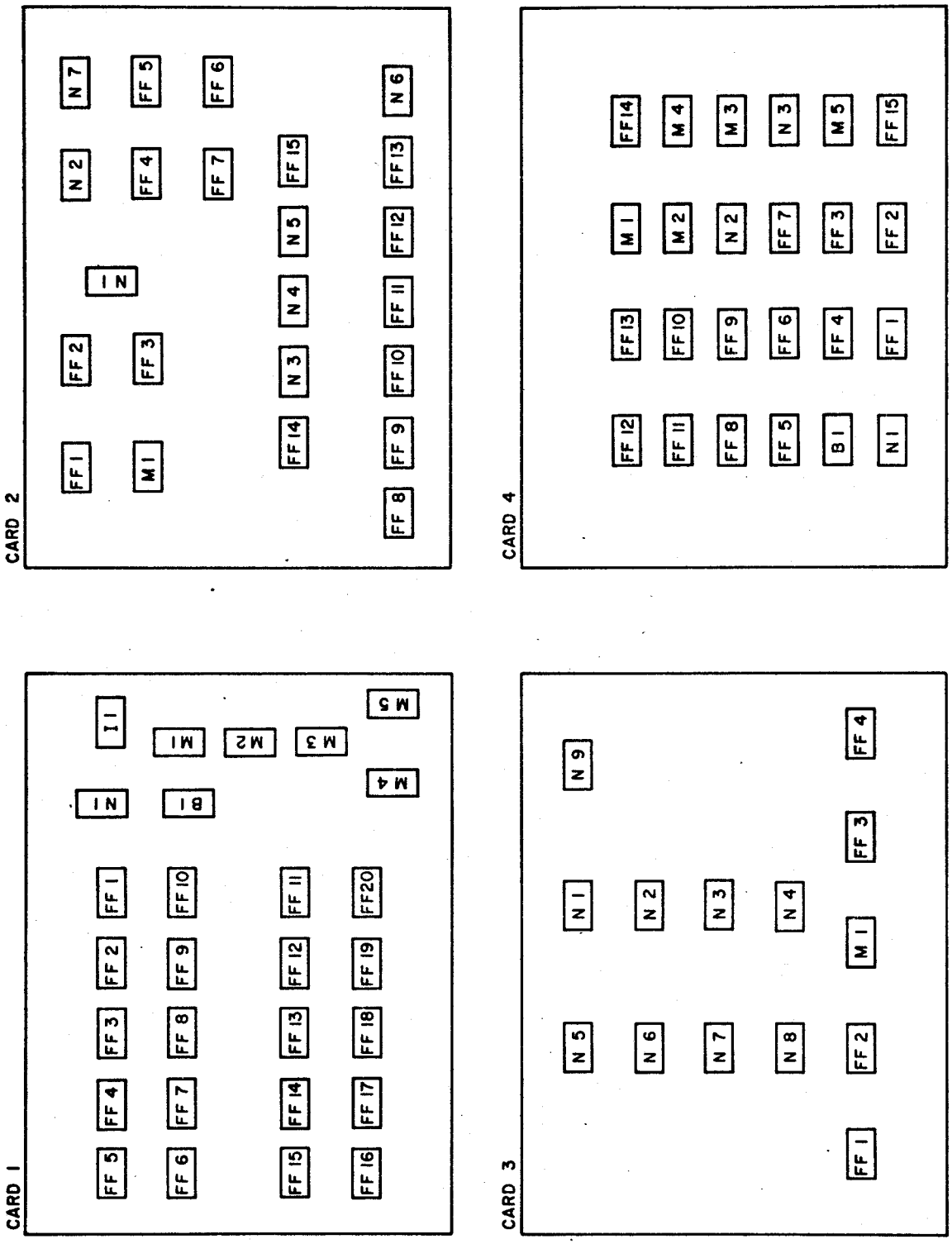
CARD 1
I1
M1
M2
M3
M5
M4
N1
B1
FF1
FF2
FF3
FF4
FF5
FF6
FF10
FF9
FF8
FF7
FF11
FF12
FF13
FF14
FF15
FF20
FF19
FF18
FF17
FF16
CARD 2
N7
FF5
FF6
N2
FF4
FF7
N1
FF2
FF3
FF1
M1
FF15
N5
N4
N3
FF14
FF13
FF12
FF11
FF10
FF9
FF8
N6
CARD 3
N9
N1
N2
N3
N4
FF4
FF3
M1
N5
N6
N7
N8
FF2
FF1
CARD 4
FF14
M4
M3
N3
M5
FF15
M1
M2
N2
FF7
FF3
FF2
FF13
FF10
FF9
FF6
FF4
FF1
FF12
FF11
FF8
FF5
B1
N1

Figure 23: Integrated circuit layout for cards 5,6,7-11 and 12.

CARD 5

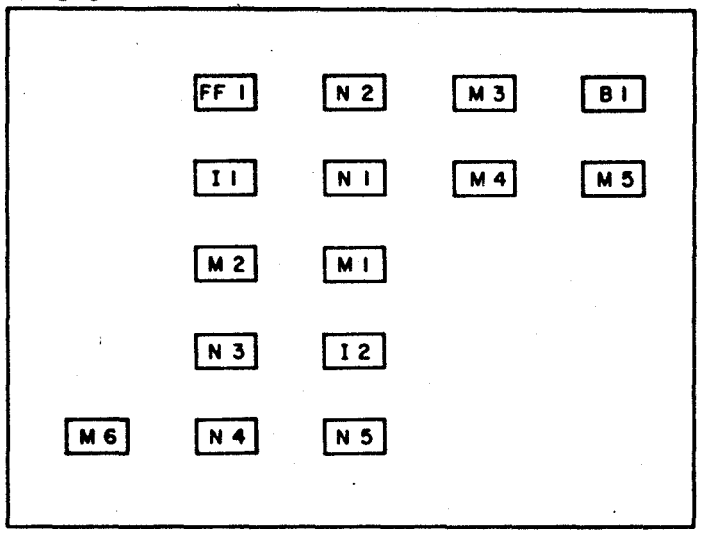

CARD 6

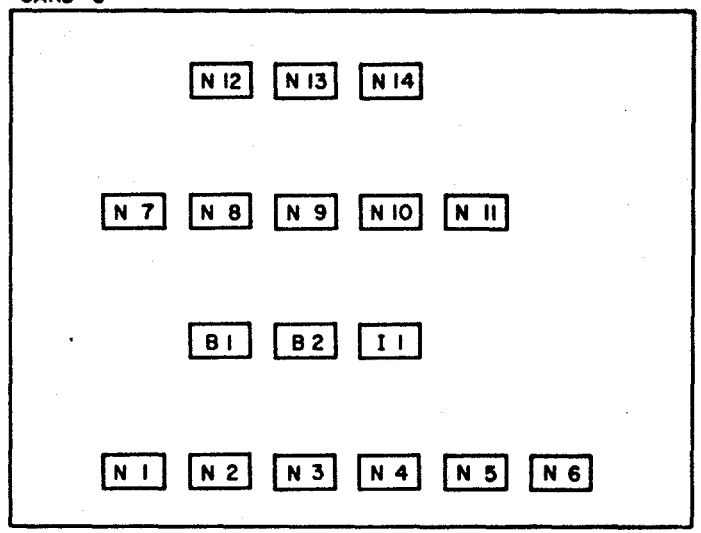

CARDS 7-11

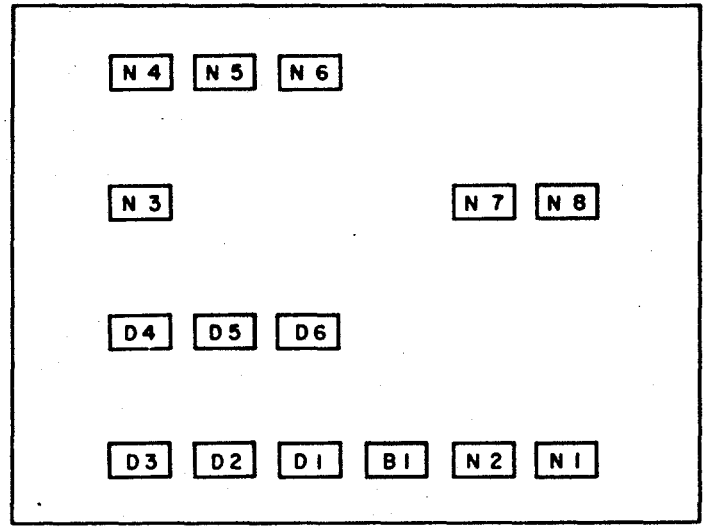

CARD 12

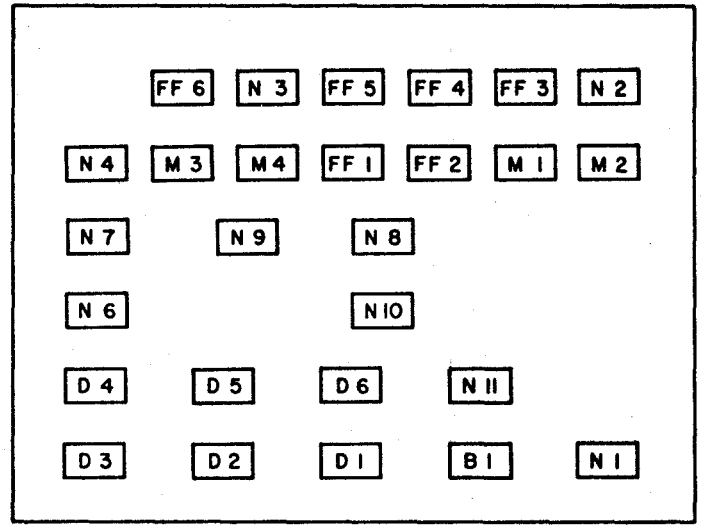

REFERENCES

Abragam, A. and Pound, R.V. 1953. Phys. Rev. 92, 943

Aeppli, H., Bishop, A.S., Frauenfelder, H., Walter, M. and Zunti, W. 1951. Phys. Rev. 82, 550.

Agarwal, Y.K., Baba, C.V.K. and Bhattacherjee, S.K. 1966. Nucl. Phys. 79, 437.

Argyle, B.E., Charap, S. and Pugh, E.W. 1963. Phys. Rev. 132, 2051.

Baranger, M. and Kumar, K. 1965. Nucl. Phys. 62, 113.

Baranger, M. and Kumar, K. 1968. Nucl. Phys. A, 110, 490.

Baranger, M. and Kumar, K. 1968. Nucl. Phys. A, 122, 241.

Beraud, R., Berkes, I., Chery, R., Haroutunian, R., Levy, M., Marest, G., Marguier, G. and Rougny, R. 1969. International Conference on Properties of Nuclear States, Montreal.

Biedenharn, L.C. and Rose, M.E. 1953. Rev. Mod. Phys. 25, 729.

Block, F. 1931. Z. Physik 61, 206.

Bruton, E.J., Cameron, J.A., Gibb. A.W., Kenyon, D.B. and Keszthelyi, L. 1969. International Conference on Properties of Nuclear States, Montreal.

Buyrn, A. and Grodzins, L. 1964. Massachusetts Institute of Technology, Progress Report 2098, No. 142.

Cameron, J.A. 1964. Can, J. Phys. 42, 1680.

Ferentz, H. and Rosenzweig, N. 1954. Argonne National Laboratory Report 5324.

Frauenfelder, H., Lawson, J.S. and Jentsckke, W. 1954. Phys. Rev. 93, 1126.

Glenn, J.E. and Saladin, J.X. 1968. Phys. Rev. Letters 20, 1298.

Grabowski, Z.W. 1969. International Conference on Properties of Nuclear States, Montreal.

Grabowski, Z.W. 1969. Phys. Rev. 183, 1019.

Keszthelyi, L., Berkes, I., Dezsi, I. and Pocs, L. 1965. Nucl. Phys. 71, 662.

Kontani, M. and Itoh, J. 1967. J. Phys. Soc. Japan 22, 345.

Kumar, K. and Baranger, M. 1966. Phys. Rev. Letters 17, 1146.

Kumar, K. and Baranger, M. 1968. Nucl. Phys. A. 122, 273.

Marshal, W. 1958. Phys. Rev. 110, 1280.

McMath, T.A. 1967. M.Sc. Thesis, McMaster University, Hamilton, Ontario.

Metzger, F.R. 1961. Nucl. Phys. 27, 612.

Mottelson, B.R. and Nilsson, S.G. 1959. Mat. Fys. Skr. Dan. Vid. Selsk 1, No. 8.

Murray, J. 1967. Ph.D. Thesis, McMaster University, Hamilton, Ontario.

Nagle, D., Frauenfelder, H., Taylor, R.D., Cochran, D.R.F. and Matthias, B.T. 1960. Phys. Rev. Letters 5, 364.

Schwartzschild, A. 1966. Phys. Rev. 141, 1206